


Cite this: *RSC Adv.*, 2025, 15, 14499

# Design and synthesis of tetrahydrochromeno[3,4-*e*]isoindole-1,3(2*H*,3*aH*)-dione derivatives *via* the Diels–Alder reaction: molecular docking, antibacterial activity, ADMET analysis and photophysical properties†

Sonali Priyadarshini Parida,<sup>a</sup> Seetaram Mohapatra,<sup>\*a</sup> Suhasini Mohapatra,<sup>id a</sup> Tankadhar Behera,<sup>b</sup> Sabita Nayak<sup>id \*a</sup> and Chita Ranjan Sahoo<sup>c</sup>

A series of fused tetrahydrochromeno[3,4-*e*]isoindole-1,3(2*H*,3*aH*)-dione derivatives was successfully synthesized *via* the Diels–Alder reaction. Molecular docking studies were conducted to understand the interaction modes between the synthesized hybrid compounds and the receptor bacterial strains of *Escherichia coli* (*E. coli*) and *Staphylococcus aureus* (*S. aureus*). Notably, the *in silico* results demonstrated that compound **19l** (−8.7 kcal mol<sup>−1</sup> with *E. coli* and −8.4 kcal mol<sup>−1</sup> with *S. aureus*) and **19p** (−8.7 kcal mol<sup>−1</sup> with *E. coli* and −9.1 kcal mol<sup>−1</sup> with *S. aureus*) exhibited good binding values. Additionally, the *in vitro* antibacterial studies showed that compounds **19l** and **19p** demonstrated excellent antibacterial activities, with a zone of inhibition (ZI) of 17 mm and a minimum inhibitory concentration (MIC) of 12.5 µg mL<sup>−1</sup> against both *E. coli* and *S. aureus*, which were comparable to the performance of the standard antibiotic ciprofloxacin. Further, the bioavailability was assessed through virtual ADMET parameters, which suggested that most of the compounds possessed favorable pharmacokinetic profiles. To further enrich the study, photophysical properties of all the synthesized molecules were also examined using UV-visible and fluorescent spectroscopies.

Received 30th March 2025

Accepted 21st April 2025

DOI: 10.1039/d5ra02212f

rsc.li/rsc-advances

## 1. Introduction

Bacterial infections have become a major problem globally.<sup>1,2</sup> The misuse and overuse of antibiotics have led to the emergence of antimicrobial resistance (AMR), resulting in rapid rise of antibiotic-resistant strains of bacteria known as.<sup>3,4</sup> Antibiotic-resistant infections result in severe illnesses, prolonged hospital stays, higher medical costs, and treatment failures. Over the past two decades, microbial infections have significantly increased.<sup>5</sup> Each year, there is a death range of approximately 70 000 worldwide due to antimicrobial resistance, and it is estimated that it may increase to 10 million cases per year by 2050.<sup>6–8</sup> Despite the discovery and development of numerous new anti-microbial drugs, there is still an increase in bacterial

infections, and their treatment is still a major challenge for public health.<sup>9,10</sup> Therefore, the discovery of novel, cost-effective antimicrobial agents is necessary to mitigate the proliferation of these pathogens.

Among the promising scaffolds for antibacterial drug development, the 2*H*-chromene core has garnered significant attention owing to its diverse biological activities.<sup>11–13</sup> Studies have demonstrated that the 2*H*-chromene derivatives exhibit potent antibacterial properties, along with other pharmacological effects such as anticancer, anti-inflammatory, anti-tubercular, and anti-HIV activities.<sup>14–23</sup> This versatile scaffold provides a robust platform for designing novel therapeutic agents with improved efficacy and selectivity against bacterial pathogens.

Similarly, maleimides are the nitrogen-containing heterocyclic motifs which have shown substantial promise in biomedical research. For instance, *N*-disubstituted maleimides represent a valuable structural motif in drug discovery, contributing to the development of novel therapeutic agents targeting bacterial infections.<sup>24–27</sup> By combining the structural features of 2*H*-chromene and maleimide, there is an opportunity to enhance antibacterial efficacy through hybrid molecules that leverage the biological potency of both scaffolds (Fig. 1).<sup>24–27</sup>

<sup>a</sup>Organic Synthesis Laboratory, Department of Chemistry, Ravenshaw University, Cuttack, 753003, Odisha, India. E-mail: seetram.mohapatra@gmail.com; sabitanayak18@gmail.com

<sup>b</sup>School of Chemistry, Sambalpur University, Jyoti Vihar, 768019, Sambalpur, Odisha, India

<sup>c</sup>ICMR-Regional Medical Research Centre, Department of Health Research, Ministry of Health & Family Welfare, Govt. of India, Bhubaneswar, 751023, Odisha, India

† Electronic supplementary information (ESI) available. CCDC 2321501. For ESI and crystallographic data in CIF or other electronic format see DOI: <https://doi.org/10.1039/d5ra02212f>



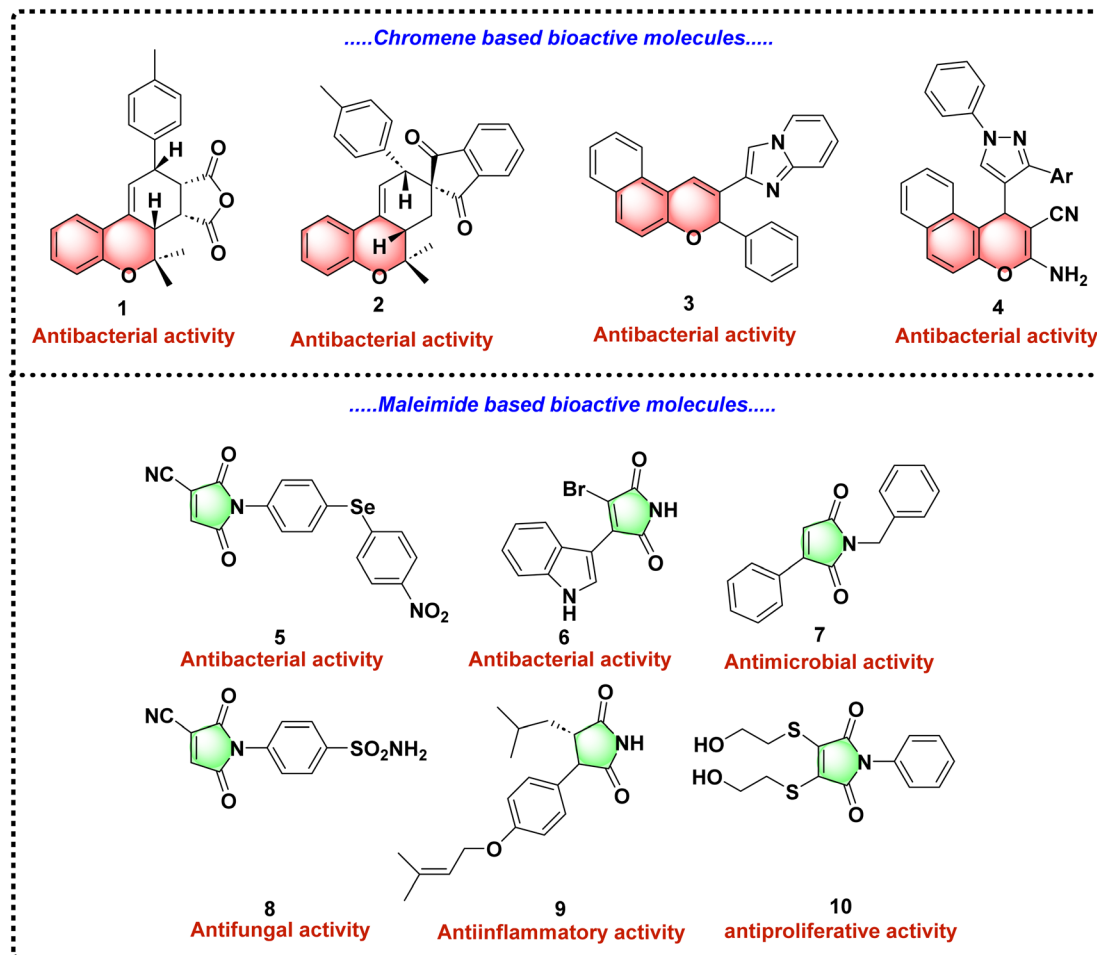
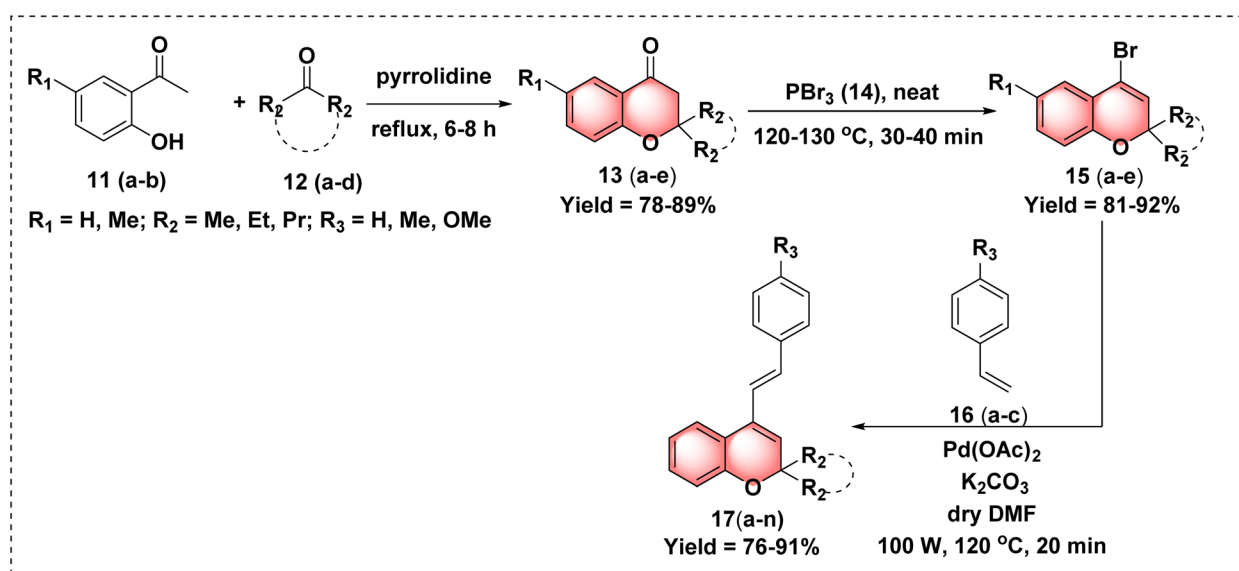


Fig. 1 Structures of some selected bioactive molecules of 2*H*-chromenes and maleimide.



Scheme 1 Synthesis of 2,2-disubstituted chromenes 13(a-e), 4-bromo-2,2-dialkylsubstituted-2*H*-chromenes 15(a-e) and 2,2-disubstituted-4-styryl-2*H*-chromene 17(a-n).

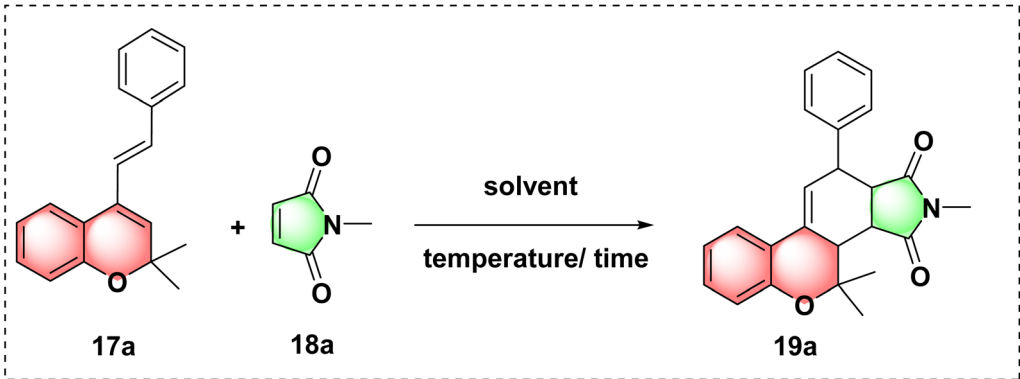


Previous studies have explored the synthesis of chromene-based maleimide hybrids using various chemical transformations. In 2006, Park *et al.* first reported the synthesis of novel benzopyran-based scaffolds through Diels–Alder reactions.<sup>28</sup> Subsequent work by the same research group in 2010 demonstrated the biological potential of these hybrids in treating prostate cancer, diabetes, and obesity.<sup>29,30</sup> However, their synthetic methods relied on expensive and carcinogenic

reagents, such as trifluoromethanesulfonic anhydride and tin catalysts, limiting their scalability and environmental compatibility.

To address these limitations and develop a more cost-effective and eco-friendly approach, we present an efficient synthesis of tetrahydrochromeno[3,4-*e*]isoindole-1,3(2*H*,3*aH*)-dione derivatives. Our strategy involves phosphorus tribromide and palladium catalyst, which are more economical and

Table 1 Exploring the reaction conditions for the Diels–Alder reaction to synthesize **19a**

					
Entry <sup>a</sup>	Maleimide equiv.	Solvent	Temp. (°C)	Time (h)	Yield (%)
1	1	DCM	35	24	12
2	2	DCM	35	24	22
3	2	THF	60	24	28
4	2	1,4-Dioxane	100	24	32
5	2	DMF	150	24	37
6	2	Benzene	80	12	51
7	2	H <sub>2</sub> O	100	24	NR
8	2	Toluene	80	12	59
9	2	Toluene	100	12	76
10	3	Toluene	120	04	91

<sup>a</sup> Reaction conditions: **17a** (1 equiv.), **18** (3 equiv.), toluene (2–3 mL); isolated yield; n.r. = no reaction.

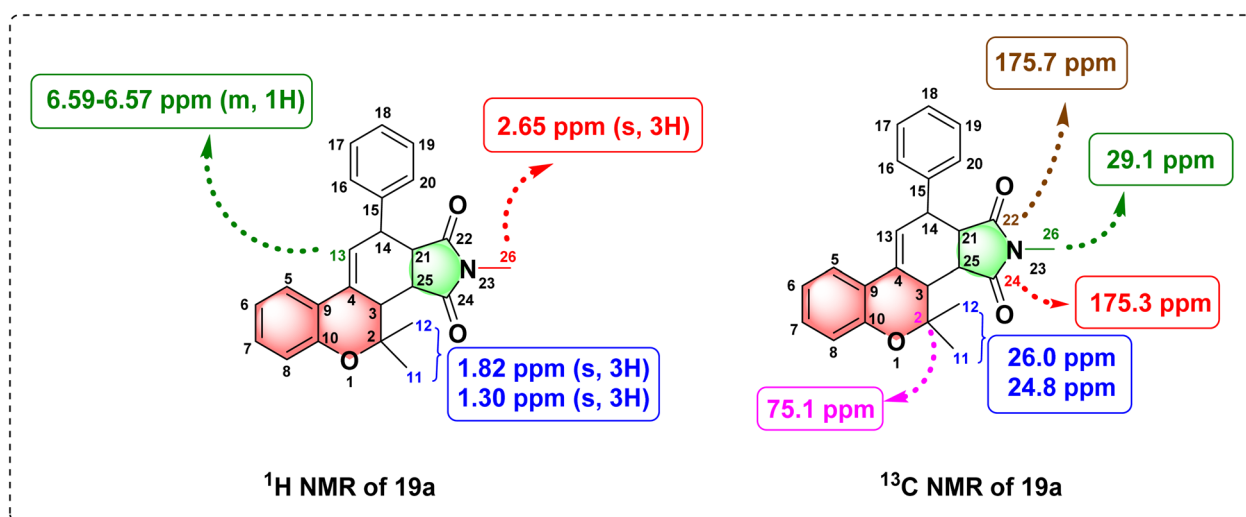
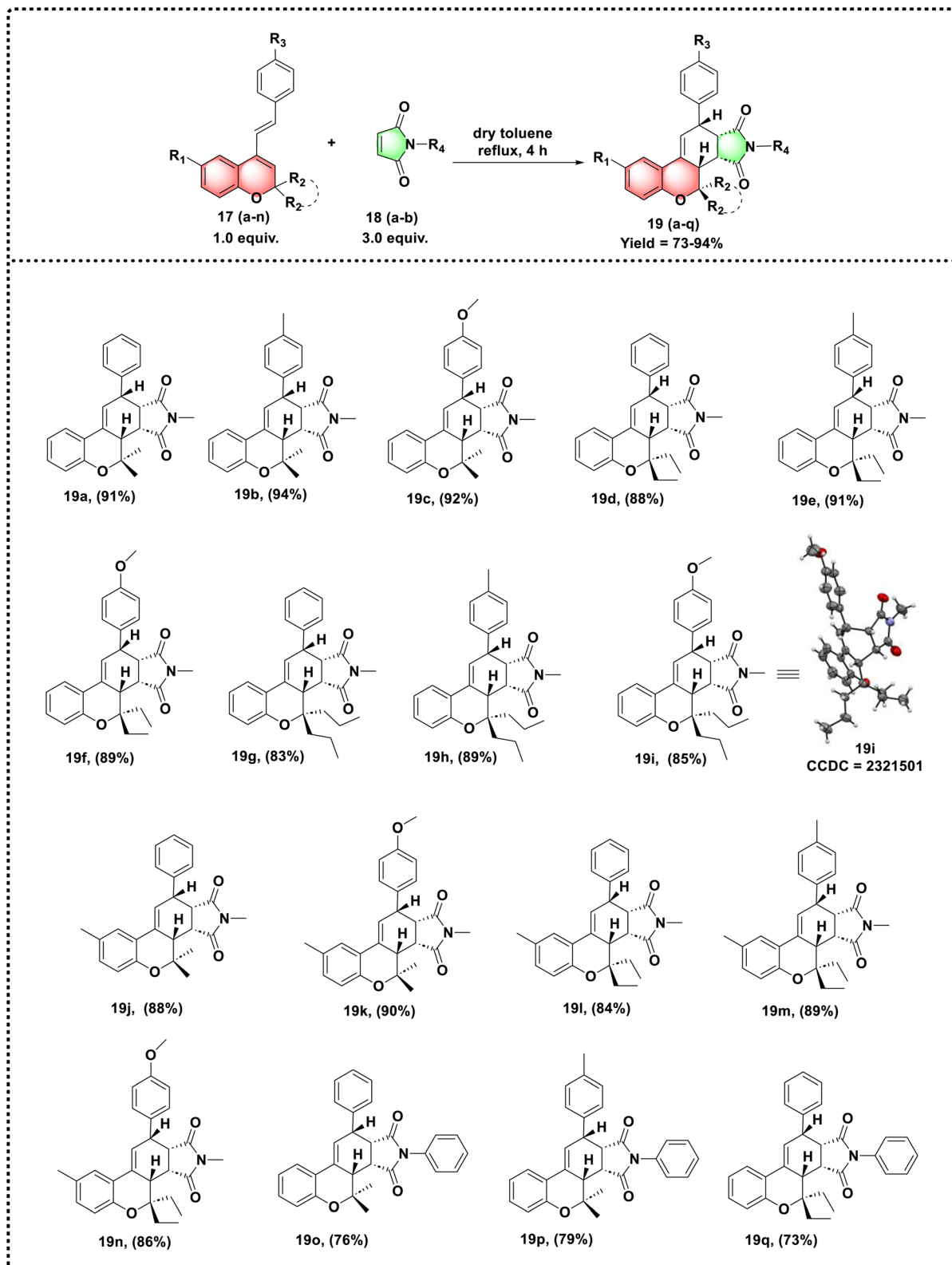


Fig. 2 <sup>1</sup>H and <sup>13</sup>C NMR spectral data analysis of compound **19a**.



Scheme 2 Synthesis of a library of tetrahydrochromeno[3,4-e]isoindole-1,3(2H,3aH)-dione derivatives **19(a-q)**.

environmentally benign alternatives. This method also explored diverse substituents on the chromene framework and the para position of the styrene ring, enhancing the scope of structural modifications.

As part of our ongoing efforts to develop tricyclic benzopyran derivatives as antibacterial agents, we recently synthesized a series of tetrahydrochromeno[3,4-e]isoindole-1,3(2H,3aH)-dione derivatives and evaluated their potent antibacterial



activities. Molecular docking studies provided insights into their binding affinities and possible mechanisms of action. Furthermore, *in silico* ADMET analyses were conducted to assess their pharmacokinetic properties, and *in vitro* antibacterial assays were performed against two pathogenic bacterial strains to evaluate their efficacy. Spectroscopic studies, including UV-visible and fluorescence analyses, were also carried out to investigate the impact of various substituents on the photophysical properties of the synthesized compounds. This comprehensive investigation aims to advance the development of potent, cost-effective antibacterial agents to combat the rising challenge of antibiotic resistance.

## 2. Result and discussion

### 2.1. Chemistry

**2.1.1 Synthesis.** Given our significant research focus on synthesizing chromene-fused six-membered carbacycles using efficient and environmentally friendly methods, our initial studies included the synthesis of the parent pharmacophore, *i.e.*, 2,2-dialkyl-4-styryl-2*H*-chromene **17a**. Our experiment began with the aldol condensation of *o*-hydroxy acetophenone **11(a-b)** and substituted ketones **12(a-d)**, followed by

intramolecular cyclization in the presence of pyrrolidine, leading to the formation of 2,2-disubstituted chromones **13(a-e)**. Treatment of  $\text{PBr}_3$  with these chromones **13(a-e)** in neat condition afforded 4-bromo-2,2-disubstituted-2*H*-chromene **15(a-e)**.<sup>31–37</sup> Having 4-bromo-2,2-dialkyl-2*H*-chromene **15(a-e)**, we intended to couple **15(a-e)** with substituted styrene **16(a-c)** to synthesize 2,2-dialkyl-4-styryl-2*H*-chromene **17(a-n)** according to the known literature method (Scheme 1).<sup>14,15</sup>

After successfully synthesizing the parent pharmacophore **17a**, we synthesized the target hybrid molecule **19a** using commercially available *N*-methyl maleimide **18a**. To synthesize the fused carbacycle **19a** through a Diels–Alder reaction, we screened the reaction conditions by altering the solvent, time and temperature.

According to the previously reported literature,<sup>14,15</sup> the reaction was first carried out in different solvents, including DCM, THF, 1,4-dioxane, DMF and benzene at their respective boiling points for about 12–24 hours, which resulted in poor to moderate yield (entries 1–6). However, the reaction did not proceed in  $\text{H}_2\text{O}$  (entry 7). We observed an increase in the product yield when the reaction temperature was raised from 80 °C to 100 °C using toluene as the solvent while maintaining the same reaction time. However, the starting materials were not fully consumed at this stage. Upon further increasing the temperature to 120 °C, we achieved excellent yield within 4 hours. This improvement may be due to the energy barrier of the reactants being overcome at higher temperatures, thereby facilitating the reaction (entries 8–10). The results are illustrated in Table 1. After the successful completion of the reaction, product **19a** was characterized using  $^1\text{H}$  NMR,  $^{13}\text{C}$  NMR and HRMS analyses.

**2.1.2 Characterization.** The structure of product **19a** was elucidated using the spectroscopic technique  $^1\text{H}$ ,  $^{13}\text{C}$  NMR and HRMS. In the proton NMR spectrum, the characteristic  $\text{H}_{13}$  proton appeared at 6.59–6.57 ppm (m, 1H). Four stereogenic  $\text{H}_3$ ,  $\text{H}_{14}$ ,  $\text{H}_{21}$  and  $\text{H}_{25}$  protons attributed to the peaks at 2.65 ppm (s, 1H), 3.73–3.70 ppm (m, 1H), 3.38–3.34 ppm (m, 1H) and 3.52–3.49 ppm (m, 1H), respectively, which clearly proved the incorporation of the maleimide ring in the 4-styryl-2*H*-chromene core. The two-methyl protons  $\text{H}_{11}$  and  $\text{H}_{12}$  appeared as two sharp singlets at 1.30 ppm and 1.82 ppm, respectively.

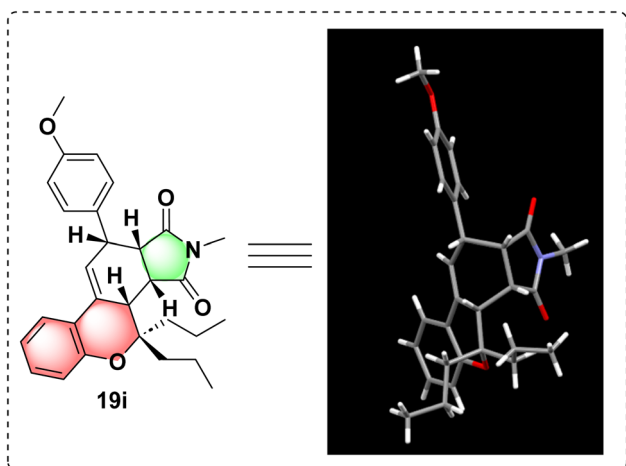
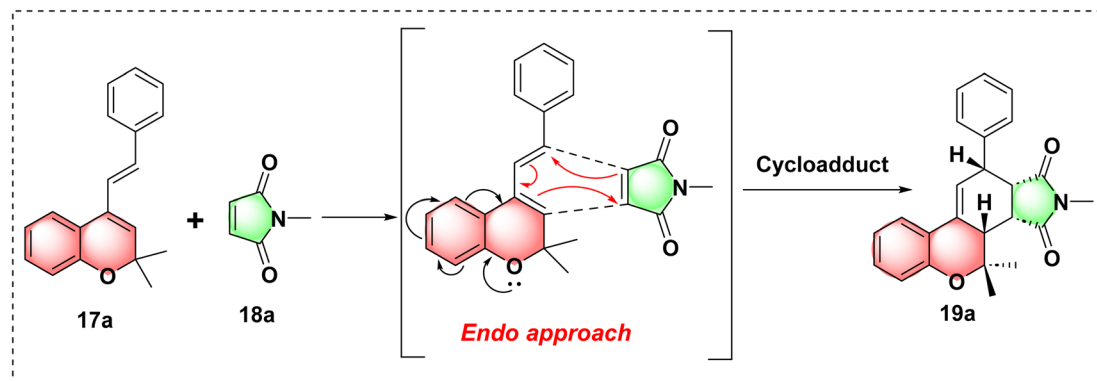
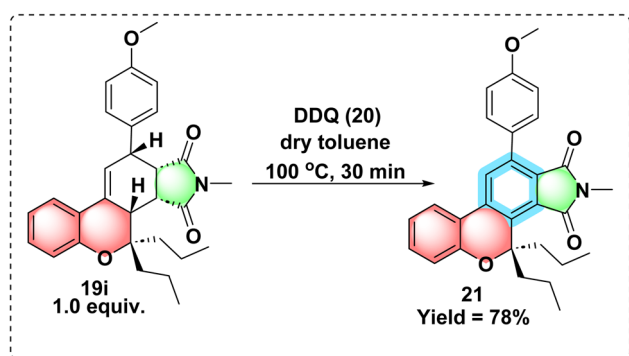


Fig. 3 Single crystal X-ray representation of compound **19i**.



Scheme 3 Proposed mechanism of **19a**.

Furthermore, the *N*-methyl proton displayed one sharp singlet at 2.65 ppm, confirming that **19a** was formed. The remaining aromatic protons appeared at their respective regions, signifying the conformation of the structure. In the  $^{13}\text{C}$  NMR, the two characteristic carbonyl carbons appeared at  $\delta$  175.7 ( $\text{C}_{22}$ ) ppm and  $\delta$  175.3 ( $\text{C}_{24}$ ) ppm, respectively. The signal at  $\delta$  29.1 ppm corresponded to the *N*-methyl carbon. Two methyl carbons of the chromene core appeared at  $\delta$  24.8 ppm and  $\delta$  26.0 ppm. The signals at the region  $\delta$  75.1 ppm represent the quaternary  $\text{C}_2$  carbon of the chromene framework and all other carbon signals resonate at appropriate positions. In the HRMS spectrum, the experimental molecular ion peak appeared at 374.1780  $[\text{M} + \text{H}]^+$ , which is equivalent to the calculated ion peak at 374.1756, confirming the formation of **19a** (Fig. 2).



Scheme 4 Synthesis of 11-(4-methoxyphenyl)-2-methyl-4,4-dipropylchromeno[3,4-e]isoindole-1,3(2*H*,4*H*)-dione **21**.

After optimizing the reaction conditions and spectroscopic characterization, we next explored the scope and generality of the reaction on various substrates, as shown in Scheme 2.

2,2-Disubstituted-4-styryl-2*H*-chromene **17(a-n)** initially reacted with *N*-methyl maleimide **18a**, resulting in tetrahydrochromeno[3,4-*e*]isoindole-1,3(2*H*,3*aH*)-dione derivatives in good to excellent yield. From Scheme 2, it is observed that the yield of the cyclized product decreases with an increase in the alkyl chain length at the  $\text{R}_2$  position of the chromene moiety. Compounds having 2,2-dimethyl substituents at the  $\text{R}_2$  position of **19(a-c)** displayed excellent yield (91–94%). Further, by modifying the methyl group to ethyl group **19(d-f)**, there is a slight decrease in the yield of the cyclized product (88–91%). Similarly, having 2,2-dipropyl substituents in **19(g-i)**, the yield decreases significantly (83–89%). However, compounds **19(j-n)** show remarkable yields (84–90%) when a methyl group is introduced at the  $\text{R}_1$  position of the chromene framework.

Furthermore, to increase the substrate scope and check the yield of the cyclized product, 2,2-disubstituted-4-styryl-2*H*-chromene **17(o-q)** was further reacted with *N*-phenyl maleimide **18b** to give the desired derivatives in good yield (73–79%). It has been concluded that *N*-methyl maleimide derivatives give higher yield as compared to *N*-phenyl maleimide, as shown in Scheme 2. The structures of cycloadducts **19(a-q)** were confirmed by  $^1\text{H}$ ,  $^{13}\text{C}$ , and HRMS spectroscopic techniques.

**2.1.3 X-ray crystallographic analysis.** The single X-ray crystallographic data is represented in Fig. 3. (CCDC-2321501), which represents the four new stereogenic protons, are in the same face.<sup>38</sup>

Table 2 Docking result scores and binding interactions of tetrahydrochromeno[3,4-*e*]isoindole-1,3(2*H*,3*aH*)-dione derivatives

Sl no.	<i>E. coli</i> (PDB ID: 3G7E)		<i>S. aureus</i> (PDBID: 3G7B)	
	Score (kcal mol <sup>−1</sup> )	Binding interactions	Score (kcal mol <sup>−1</sup> )	Binding interactions
<b>19a</b>	−7.1	Arg62, Ala39, Pro65, Lys89	−8.1	Ile79, Ile63, Ala38
<b>19b</b>	−6.2	Asn32, Phe90, Ile80, Ala76, Pro65, Ile64	−7.8	Asn31, Ile63, Ala38
<b>19c</b>	−7.9	Pro65, Asp35, Phe90, His102, Ala39, Lys89, Ile64, Ala76, Ile80	−8.2	Arg61, Ser32, Ala38, Asn31, Ile79, Pro64, Ile63
<b>19d</b>	−7.9	Arg62, Pro65, Lys89, Ala39, Ile64	−8.3	Asn31, Pro64
<b>19e</b>	−7.4	Arg62, Leu38, Lys89, Val97	−8.3	Asn31, Glu35, Arg61, Ile63, Ala38
<b>19f</b>	−6.5	Phe90, Arg62, Leu38, Pro65, Ala39, Lys89	−7.0	Asn31, Glu35, Pro64, Ile79, Ile63, Ala75
<b>19g</b>	−6.7	Arg62, Leu38, His41, Ala39, Lys89	−7.9	Glu35, Arg61, Ile79, Ile63, Pro64
<b>19h</b>	−5.6	Phe90, Glu36, Arg62, Ile80, Pro65, Ile64, Ala39, Lys89	−7.9	Arg61, Ile63, Ile79, Pro64, Ala38
<b>19i</b>	−8.2	Asp35, Pro65, Ile64, Ile80, Leu38, Ala39, Lys89	−6.9	Asn31, Pro64, Ile63
<b>19j</b>	−6.9	Leu38, Glu36, Lys89, Ala39, Asp35, Val97	−9.1	Glu35, Arg61, Asn31, Ile63, Ile79, Ile129, Pro64
<b>19k</b>	−6.9	Ala39, Arg62, Glu36, Pro65, Ala39	−8.2	Arg61, Ile63, Ile79, Ala38
<b>19l</b>	−8.7	Thr151, Ile64, Pro65, Ala33, Glu36, Arg62, Phe90, Lys89, Ala39, Ile80	−8.4	Asn31, Arg61, Ile79, Pro64, Ile63, Ala38
<b>19m</b>	−7.1	Arg62, Glu36, Asp35, Lys89, His102, Ala39	−8.4	Asn31, Arg61, Glu35, Gly62, Pro64, Ile63
<b>19n</b>	−8.3	Arg62, Ala86, Asp59, Lys89, Val106, Val29, Ala33, Ile64, Pro65, Ile80	−8.4	Asn31, Ile79, Ile63
<b>19o</b>	−6.4	Arg62, Lys89, Asn32, Pro65, Ile64, Phe90	−8.6	Arg61, Ile63, Asn31, Ile79, Pro64
<b>19p</b>	−8.7	Arg62, Val97, Lys89, Ala39, Ile64, Pro65	−9.1	Asn31, Glu35, Arg61, Ile63, Ile79, Pro64
<b>19q</b>	−7.5	Arg62, Glu36, Asp35, Ala39, Lys89, Val97	−8.7	Glu35, Arg61, Ile79, Ile63, Pro64





**2.1.4 Plausible mechanism.** The plausible mechanism of 2,4,4-trimethyl-11-phenyl-3*b*,4,11,11*a*-tetrahydrochromeno[3,4-*e*]isoindole-1,3(2*H*,3*aH*)-dione **19a** is shown in Scheme 3. The Diels–Alder reaction between 2,2-dimethyl-4-styryl-2*H*-chromene **17a** with *N*-methyl maleimide **18a** yields a six-membered ring with four stereocenters. In the Diels–Alder reaction, the endo approach predominates over the exo approach due to secondary interactions; hence, we presumed the stereochemistry of four stereogenic hydrogens are in the same face and the plane of ring is influenced by the endo approach of the dienophile with diene in a transition state.

**2.1.5 Transformations of 11-(4-methoxyphenyl)-2-methyl-4,4-dipropyl-3*b*,4,11,11*a*-tetrahydrochromeno[3,4-*e*]isoindole-1,3(2*H*,3*aH*)-dione **19i**.** To demonstrate the synthetic utility of our designed molecule from previously described methods,<sup>39</sup> we proposed a derivatization reaction, as described in Scheme 4. Initially, the cyclo-adduct 11-(4-methoxyphenyl)-2-methyl-4,4-

dipropyl-3*b*,4,11,11*a*-tetrahydrochromeno[3,4-*e*]isoindole-1,3(2*H*,3*aH*)-dione **19i** reacted with DDQ (2,3-dichloro-5,6-dicyano-1,4-benzoquinone) (1.5 equiv.) in the presence of toluene at 100 °C for 30 min to afford the aromatized product 11-(4-methoxyphenyl)-2-methyl-4,4-dipropylchromeno[3,4-*e*]isoindole-1,3(2*H*,4*H*)-dione **21** in excellent yield. After the synthesis and confirmation of the structure from <sup>1</sup>H NMR, <sup>13</sup>C NMR and HRMS spectroscopic techniques, we further progressed to study the *in silico* and *in vitro* antimicrobial activity and ADMET study of all the synthesized cyclized products **19(a–q)**.

## 3. Biological studies

### 3.1. Molecular docking study

Molecular docking studies of the synthesized hybrid tetrahydrochromeno[3,4-*e*]isoindole-1,3(2*H*,3*aH*)-dione **19(a–q)**

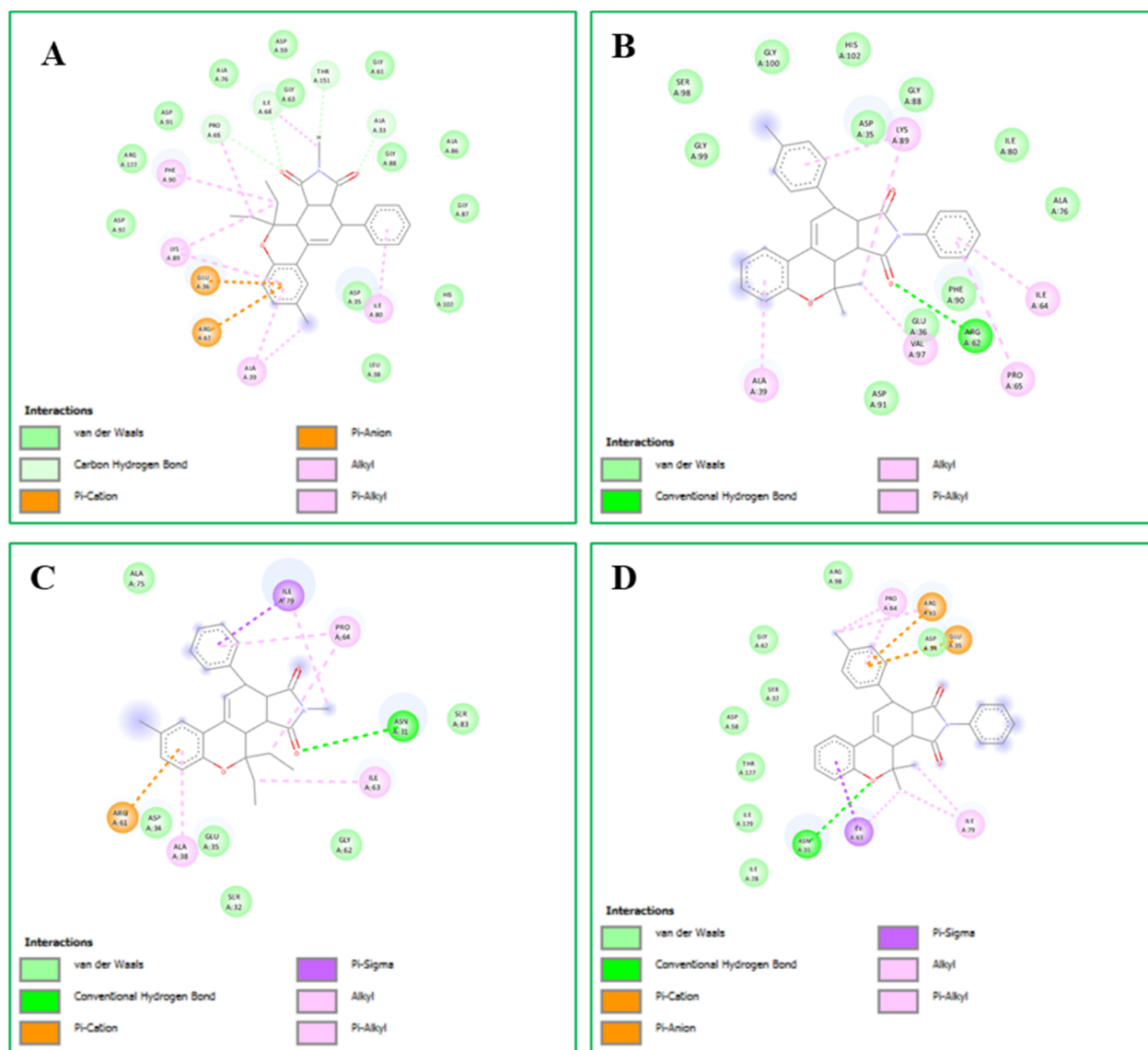


Fig. 4 2D interactions of the most potent compounds (A) compound **19i** and (B) Compound **19p** with Gram-negative bacterial DNA gyrase (PDBID: 3 G7E). (C) Compound **19i** and (D) compound **19p** with Gram-positive bacterial DNA gyrase (PDBID: 3G7B).

derivatives were performed to identify the binding interaction with the DNA gyrase inhibitor. The Gram-negative bacterial strain *E. coli* and Gram-positive bacterial strain *S. aureus* are two human pathogenic bacterial strains of the DNA gyrase inhibitor used for molecular modelling. The crystal structure of *E. coli* (PDB ID: 3G7E) and *S. aureus* (PDBID: 3G7B) were retrieved, and the heteroatoms and water molecules were removed during the docking procedure. Autodock tool 4.2.0 was used to determine the binding affinity scores, and the Discovery Studio v 2017 program was employed in visualizing the intermolecular binding interaction of the docked complex. In this study, seventeen newly designed hybrid molecules were successfully docked, and the binding affinity values ranged from  $-5.6 \text{ kcal mol}^{-1}$  to  $-8.7 \text{ kcal mol}^{-1}$  in the case of *E. coli* and  $-6.9 \text{ kcal mol}^{-1}$  to  $-9.1 \text{ kcal mol}^{-1}$  in the case of *S. aureus*. The current investigation revealed that compound **19l** possessing diethyl at the  $R_2$  position of the chromene ring, methyl at the  $R_1$  position, hydrogen at the  $R_3$  position and methyl at the  $R_4$  position showed very good yield  $-8.7 \text{ kcal mol}^{-1}$  with *E. coli* DNA gyrase and  $-8.4 \text{ kcal mol}^{-1}$  with *S. aureus* DNA gyrase. Furthermore, compound **19p** possesses dimethyl at the  $R_2$

position of the chromene ring, methyl at the  $R_3$  position and phenyl group at the  $R_4$  position, demonstrating robust binding interactions with a binding energy value of  $-8.7 \text{ kcal mol}^{-1}$  for *E. coli* (PDB ID: 3G7E) and  $-9.1 \text{ kcal mol}^{-1}$  for *S. aureus* (PDBID: 3G7B). The synthesized compounds interacted with bacterial DNA gyrase through various interactions such as van der Waals, conventional hydrogen bond, carbon-hydrogen bond, alkyl,  $\pi$ -alkyl,  $\pi$ -anion,  $\pi$ -cation, and  $\pi$ -sigma. The docking scores and their binding interactions are displayed in Table 2.

From Table 2, it is noted that compound **19l** has very good binding interactions with the active pocket site of *E. coli* and *S. aureus* DNA gyrase. The docked complex with DNA gyrase *E. coli* displays a series of van der Waals interactions with specific amino acid residues Asp92, Arg122, Asp91, Ala76, Asp59, Gly63, Gly61, Gly88, Ala86, Gly87, His102, Asp35, Leu38, carbon hydrogen bonds with Pro65, Thr151, Ile64, Ala33,  $\pi$ -cation and  $\pi$ -anion interactions with Arg62, Glu36, alkyl interaction with Ala39, Phe90, Lys89, Pro65, Ile64, and  $\pi$ -alkyl interaction with Ile80, Ala39, Lys89 for compound **19l**. Similarly, compound **19l** held into the active cavities with the DNA gyrase enzymes of *S. aureus* (PDBID: 3G7B) via van der Waals interactions with Ala75,

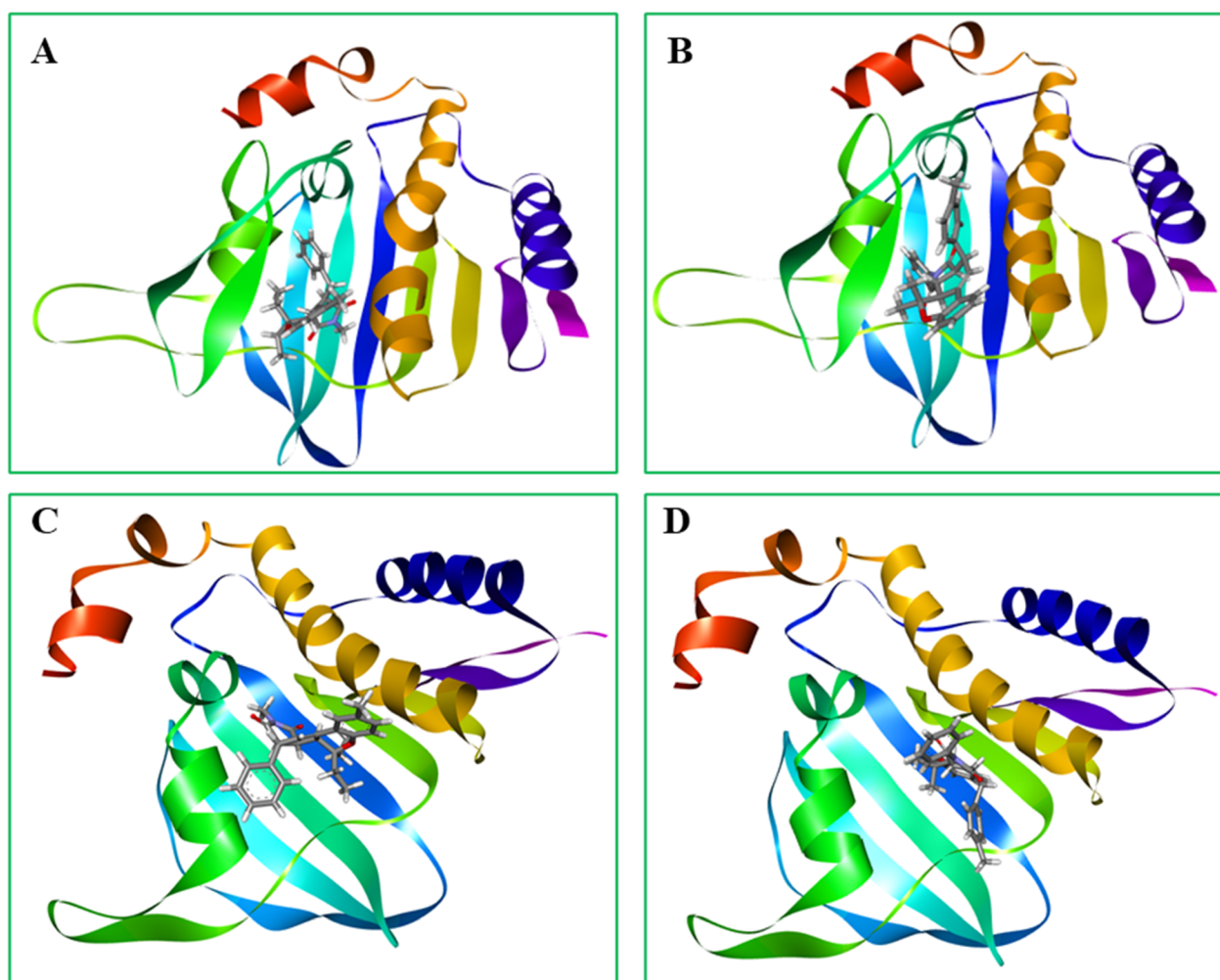


Fig. 5 Most potent molecular docking studies of maleimide derivatives. The images depict the protein and ball-stick models. (A) Compound **19l** and (B) compound **19p** with Gram-negative bacterial DNA gyrase (PDBID: 3G7E). (C) Compound **19l** and (D) Compound **19p** with Gram-positive bacterial DNA gyrase (PDBID: 3G7B).





Asp34, Glu35, Ser32, Gly62, Ser83, conventional hydrogen bond with Asn31,  $\pi$ -cation interaction with Arg61,  $\pi$ -sigma interaction with Ile79, alkyl interaction with Ile63, Pro64 and  $\pi$ -alkyl interaction with Ala38, Ile63 and Pro64. Compound **19p** also displayed a remarkable result for both the docked complexes: van der Waals interactions with Gly99, Ser98, Gly100, His102, Asp35, Gly88, Ile80, Ala76, Phe90, Glu36, Asp91, conventional hydrogen bond with Arg62, alkyl interaction with Val97, Lys89,  $\pi$ -alkyl interaction with Ala39, Pro65, Ile64 in the case of *E. coli* DNA gyrase. Alternatively, *S. aureus* shows van der Waals interactions

with Arg98, Gly62, Ser32, Asp58, Thr127, Ile129, Ile28, Asp34, conventional hydrogen bond with Asn31,  $\pi$ -cation and  $\pi$ -anion interactions with Arg61, Glu35,  $\pi$ -sigma with Ile63, alkyl and  $\pi$ -alkyl interaction with Ile79 and Pro64 for compound **19p**. From the docking score, it is observed that the compounds **19l** and **19p** display promising results in terms of antibacterial activities. The 2D and 3D diagrams of the most potent compounds, **19l** and **19p**, against *E. coli* DNA gyrase and *S. aureus* DNA gyrase, are represented in Fig. 4 and 5, respectively.

### 3.2. Antibacterial evaluation

A series of tetrahydrochromeno[3,4-*e*]isoindole-1,3(2*H*,3*aH*)-dione derivatives **19(a-q)** were investigated for *in vitro* antibacterial activities against two human bacterial strains. All the synthesized derivatives were evaluated against Gram-negative *E. coli* and Gram-positive *S. aureus* via the agar well diffusion method using the standard drug ciprofloxacin. The ZI (zone of inhibition) and MIC (minimum inhibitory concentration) values of those molecules against these bacteria are also determined and the molecules are found to be active against both the bacterial strains, as represented in Table 3.

Among all the tested compounds, compound 4,4-diethyl-2,8-dimethyl-11-phenyl-3*b*,4,11,11*a*-tetrahydrochromeno[3,4-*e*]isoindole-1,3(2*H*,3*aH*)-dione **19l** and 4,4-dimethyl-2-phenyl-11-(*p*-tolyl)-3*b*,4,11,11*a*-tetrahydrochromeno[3,4-*e*]isoindole-1,3(2*H*,3*aH*)-dione **19p** were found to be the most potent compounds with a ZI of 17 mm against both *E. coli* and *S. aureus* bacterial strains. Furthermore, we performed a cell viability assay to determine the minimum inhibitory concentration (MIC) of the compounds. The MIC results revealed that both *E. coli* and *S. aureus* displayed potent activity with an MIC value of 12.5  $\mu\text{g mL}^{-1}$  for both compounds **19l** and **19p**. However, from the antibacterial study, we found that compound 2-methyl-4,4-dipropyl-11-(*p*-tolyl)-3*b*,4,11,11*a*-tetrahydrochromeno[3,4-*e*]isoindole-1,3(2*H*,3*aH*)-dione **19h**

**Table 3** Antibacterial activities of the newly synthesized tetrahydrochromeno[3,4-*e*]isoindole-1,3(2*H*,3*aH*)-dione derivatives **19(a-q)**. (Abbreviations: ZI, zone of inhibition; MIC, minimum inhibitory concentration. \*Standard drug: ciprofloxacin)

Sl. no.	<i>E. coli</i>		<i>S. aureus</i>	
	ZI (mm)	MIC ( $\mu\text{g mL}^{-1}$ )	ZI (mm)	MIC ( $\mu\text{g mL}^{-1}$ )
<b>19a</b>	15	25	16	25
<b>19b</b>	13	50	15	25
<b>19c</b>	16	25	16	25
<b>19d</b>	16	25	16	25
<b>19e</b>	15	25	16	25
<b>19f</b>	14	50	14	50
<b>19g</b>	14	50	15	25
<b>19h</b>	12	50	15	25
<b>19i</b>	16	50	14	50
<b>19j</b>	14	50	17	12.5
<b>19k</b>	14	50	16	25
<b>19l</b>	17	12.5	17	12.5
<b>19m</b>	15	25	16	25
<b>19n</b>	16	25	16	25
<b>19o</b>	14	50	17	12.5
<b>19p</b>	17	12.5	17	12.5
<b>19q</b>	15	25	16	25
Std Ciprofloxacin	—	6.25	—	6.25

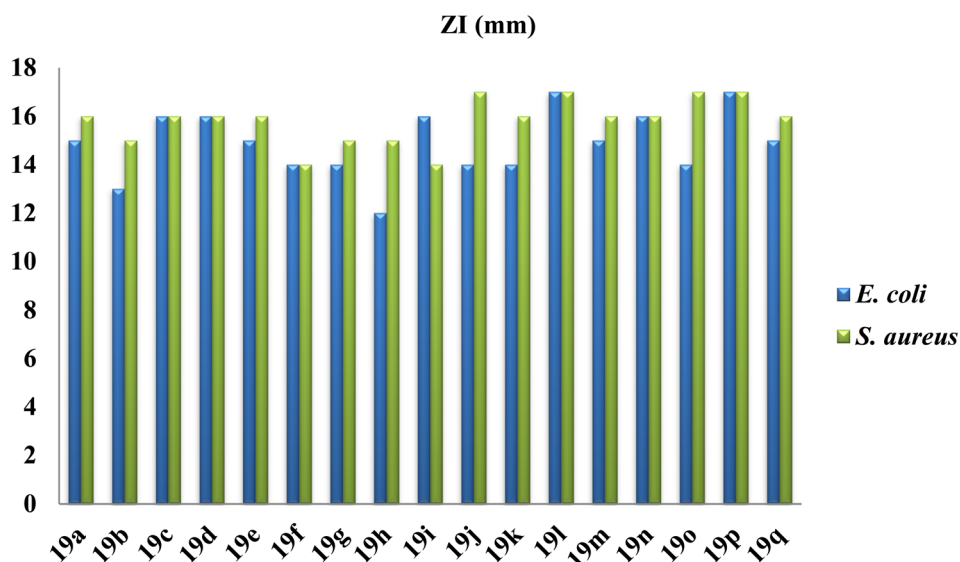


**Fig. 6** Graphical representation of the *in vitro* antimicrobial (ZI) assay of the synthesized tetrahydrochromeno[3,4-*e*]isoindole-1,3(2*H*,3*aH*)-dione derivatives.



possessed notably poor antimicrobial activity with a ZI value of 12 mm and 15 mm for *E. coli* and *S. aureus*, respectively. The respective ZI values and MIC values of all the tested compounds are illustrated graphically in Fig. 6 and 7, respectively.

### 3.3. Structure activity relationship (SAR) studies

From the *in silico* molecular docking study, we found that compounds, 4,4-diethyl-2,8-dimethyl-11-phenyl-3*b*,4,11,11*a*-tetrahydrochromeno[3,4-*e*]isoindole-1,3(2*H*,3*aH*)-dione **19l** and 4,4-dimethyl-2-phenyl-11-(*p*-tolyl)-3*b*,4,11,11*a*-tetrahydrochromeno[3,4-*e*]isoindole-1,3(2*H*,3*aH*)-dione **19p**, have good binding scores of  $-8.7 \text{ kcal mol}^{-1}$  and  $-8.7 \text{ kcal mol}^{-1}$  for *E. coli* and  $-8.4 \text{ kcal mol}^{-1}$  and  $-9.1 \text{ kcal mol}^{-1}$  for *S. aureus* DNA gyrase, respectively. It also demonstrated effective antibacterial activity with a MIC value of  $12.5 \mu\text{g mL}^{-1}$  against both *E. coli* and *S. aureus* bacterial strains for both molecules **19l** and **19p**. Furthermore, it is observed that compound 2-methyl-4,4-dipropyl-11-(*p*-tolyl)-3*b*,4,11,11*a*-tetrahydrochromeno[3,4-*e*]isoindole-1,3(2*H*,3*aH*)-dione **19h** tivity with a MIC value of  $50 \mu\text{g mL}^{-1}$  for *E. coli* and  $25 \mu\text{g mL}^{-1}$  for *S. aureus* bacterial strains. Also, compound **19h** has a poor binding affinity score ( $-5.6 \text{ kcal mol}^{-1}$  for *E. coli* and  $-7.9 \text{ kcal mol}^{-1}$  for *S. aureus*), as compared to all the synthesized molecules.

The structure–activity relationship studies reveal that the compound is more favorable towards antibacterial activity, particularly when the chromene scaffold is associated with a diethyl group at the  $R_2$  position with a methyl group at the  $R_1$

position, hydrogen at the  $R_3$  position with *N*-methyl maleimide (**19l**) as well as with dimethyl at the  $R_2$  position, methyl at the  $R_3$  position with *N*-phenyl maleimide (**19p**). However, very poor results were observed in the case of compound **19h**, which is associated with the dipropyl group at the  $R_2$  position and methyl at the  $R_3$  position with *N*-methyl maleimide. The pictorial representation of the SAR study is illustrated in Fig. 8.

### 3.4. Estimation of physicochemical, pharmacokinetic and ADMET properties

The *in silico* pharmacokinetic study using ADMET was carried out for drug development cascades. The pharmacokinetic and physicochemical properties of seventeen synthesized molecules **19(a–q)** were evaluated using the SwissADME tool, comparing them to the standard drug ciprofloxacin.<sup>40,41</sup> Subsequently, the Lipinski's Rule of Five (RO5) was used for the physicochemical properties.<sup>42</sup> It states that molecular weight (MW) should be  $\leq 500 \text{ g mol}^{-1}$ , octanol–water partition coefficient (cLog *P*) should be  $\leq 5$ , number of hydrogen bond acceptors (HBA) should be  $\leq 10$ , number of hydrogen bond donors (HBD) should be  $\leq 5$  and topological polar surface area (TPSA) should be  $\leq 140 \text{ \AA}^2$  for a potential compound to be an orally active drug molecule.<sup>43–45</sup>

Additionally, the topological polar surface area (TPSA), which is inversely related to the percentage absorption (%ABS =  $109 - 0.345 \times \text{TPSA}$ ), was proposed as a potential alternative to counting hydrogen bonding groups for estimating the

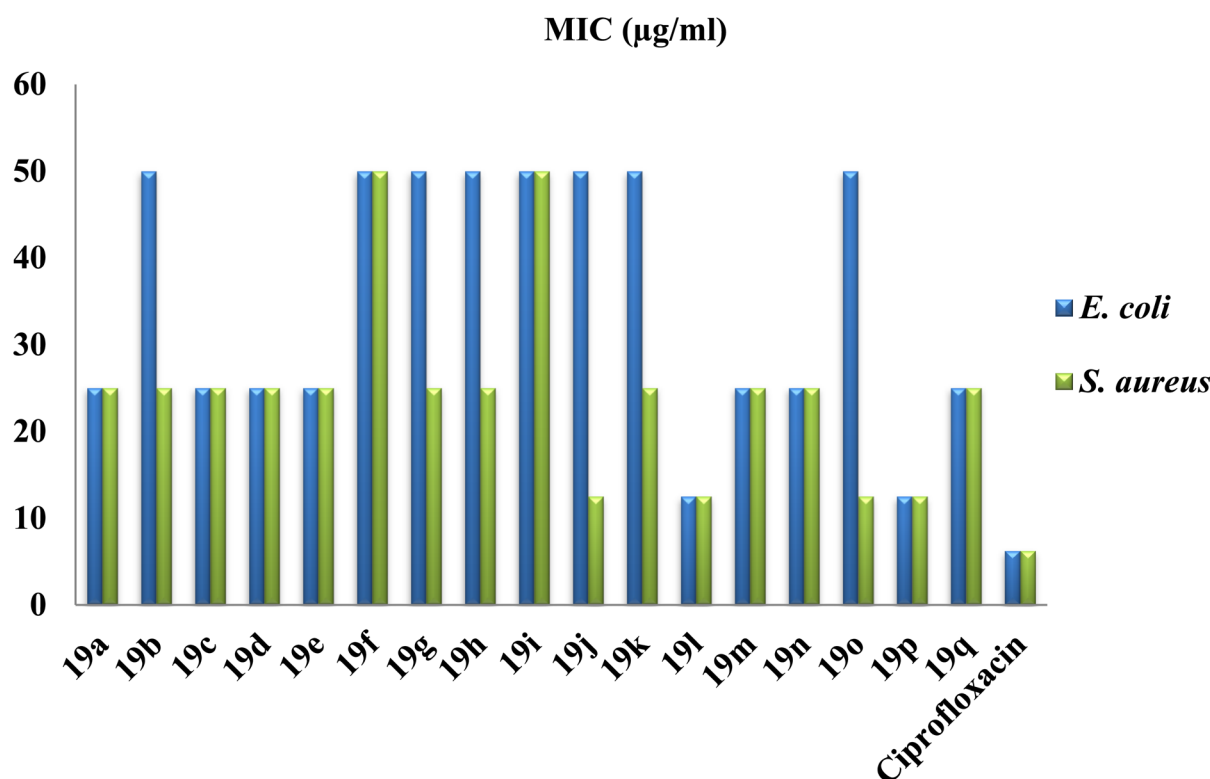


Fig. 7 Graphical representation of the *in vitro* antimicrobial (MIC) assay of the synthesized tetrahydrochromeno[3,4-*e*]isoindole-1,3(2*H*,3*aH*)-dione derivatives compared with the standard drug ciprofloxacin.



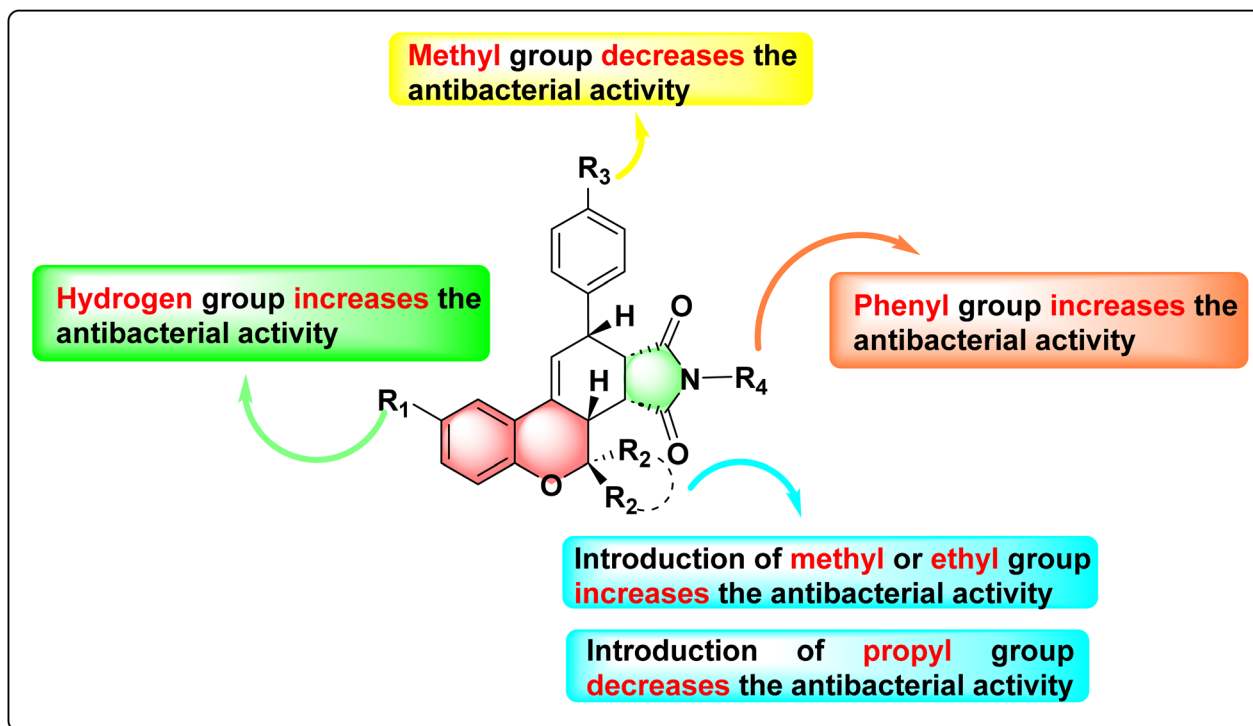


Fig. 8 Pictorial representation of the SAR of the tetrahydrochromeno[3,4-e]isoindole-1,3(2H,3aH)-dione derivatives **19(a–q)**.

absorption percentages. The analysis of the results indicates that the synthesized derivatives exhibit favorable physico-chemical properties, with hydrogen bond acceptors (HBA) ranging from 3 to 4, TPSA values between 36.13 and 44.06 Å, and an acceptable number of hydrogen bond donors.

Again, the toxicity of the potent molecules **19l** and **19p** was determined using ProTox II online software. ProTox II tool

determines the toxicity levels and the 50% lethal dose (LD<sub>50</sub>).<sup>20,46–48</sup> From Table 4, compound **19l** showed a Class 5 toxicity level with an estimated LD<sub>50</sub> of 2200 mg kg<sup>−1</sup>, whereas compound **19p** showed a Class 5 toxicity level with an estimated LD<sub>50</sub> of 3900 mg kg<sup>−1</sup> (Fig. 9). Consequently, the blood–brain-barrier (BBB), human-intestinal-absorption (HIA), and Caco-2-permeability were evaluated. From the result, it was

Table 4 Calculation of Lipinski's 'rule of 5' for the tetrahydrochromeno[3,4-e]isoindole-1,3(2H,3aH)-dione derivatives **19(a–q)**

Sl. no	Compound code	RO5						Toxicity		Pharmacokinetics		
		MW <sup>a</sup>	HBA <sup>b</sup>	HBD <sup>c</sup>	mlogP <sup>d</sup>	TPSA <sup>e</sup>	% ABS <sup>f</sup>	Class	LD <sub>50</sub> <sup>g</sup> (mg kg <sup>−1</sup> )	BBB <sup>h</sup>	HIA <sup>i</sup>	Caco-2 <sup>j</sup>
1	<b>19a</b>	373	3	0	3.69	36.13	96.53	5	2200	0.93	1	0.63
2	<b>19b</b>	387	3	0	4.13	36.13	96.53	5	2200	0.93	1	0.63
3	<b>19c</b>	403	4	0	3.65	43.67	93.93	5	2200	0.87	1	0.60
4	<b>19d</b>	401	3	0	4.35	36.52	96.40	5	2200	0.97	1	0.63
5	<b>19e</b>	415	3	0	4.79	36.52	96.40	5	2200	0.97	1	0.63
6	<b>19f</b>	431	4	0	4.31	44.06	93.79	5	2200	0.93	1	0.60
7	<b>19g</b>	429	3	0	5.37	36.52	96.40	5	2200	0.98	1	0.63
8	<b>19h</b>	443	3	0	5.81	36.52	96.40	5	2200	0.98	1	0.63
9	<b>19i</b>	459	4	0	5.32	44.06	93.79	5	2200	0.97	1	0.60
10	<b>19j</b>	387	3	0	4.13	36.13	96.53	5	2200	0.93	1	0.63
11	<b>19k</b>	417	4	0	4.09	43.67	93.93	5	2200	0.87	1	0.60
12	<b>19l</b>	415	3	0	4.79	36.52	96.40	5	2200	0.97	1	0.63
13	<b>19m</b>	429	3	0	5.24	36.52	96.40	5	2200	0.97	1	0.63
14	<b>19n</b>	445	4	0	4.75	44.06	93.79	5	2200	0.93	1	0.60
15	<b>19o</b>	435	3	0	4.98	35.48	96.75	5	3900	0.95	1	0.59
16	<b>19p</b>	449	3	0	5.42	35.48	96.75	5	3900	0.94	1	0.58
17	<b>19q</b>	463	3	0	5.64	35.87	96.62	5	3900	0.98	1	0.61
18	Ciprofloxacin	331	5	2	1.28	74.57	83.27	4	1000	0.72	0.97	0.64

<sup>a</sup> Molecular weight in g mol<sup>−1</sup>. <sup>b</sup> Number of H-bond acceptors. <sup>c</sup> Number of H-bond donors. <sup>d</sup> Partition coefficient (lipophilicity). <sup>e</sup> Topological polar surface area in Å. <sup>f</sup> % of Absorbance. <sup>g</sup> 50% lethal dose. <sup>h</sup> Blood brain barrier permeant. <sup>i</sup> Human-intestinal-absorption. <sup>j</sup> Caco-2-permeability.



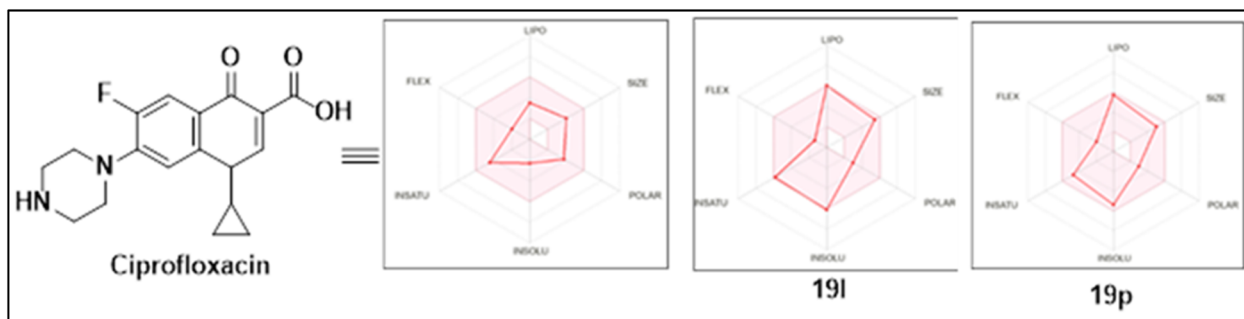


Fig. 9 Bioavailability radar plot of the standard antibiotic ciprofloxacin compared with synthesized compounds **19l** and **19p**.

concluded that most of the compounds are less toxic and suitable as oral bioactive drug molecules.

A radar chart was plotted to describe the six physicochemical parameters: lipophilicity (LIPO), size (SIZE), polarity (POLAR), solubility (INSOLU), saturation (INSATU), and flexibility (FLEX). As illustrated in Fig. 9, the physicochemical properties of compounds **19l** and **19p** generally fall within the acceptable range (pink region) (Fig. 10).<sup>2,49</sup>

After the ADMET analysis, from the literature survey, we found that both 2*H*-chromene and maleimide show fluorescent behavior.<sup>50–52</sup> Hence, we studied the UV and fluorescence activity of all the synthesized tetrahydrochromeno[3,4-*e*]isoindole-1,3(2*H*,3*aH*)-dione derivatives **19(a–q)**.

## 4. Photophysical properties

### 4.1. UV-visible studies

The UV-visible spectra of seventeen synthesized tetrahydrochromeno[3,4-*e*]isoindole-1,3(2*H*,3*aH*)-dione derivatives **19(a–q)** were recorded in a Shimadzu single monochromator UV-2600 spectrophotometer at 15  $\mu$ M concentration. Initially, the cyclic derivative **19a** was dissolved in DMSO at 15  $\mu$ M concentration, and the spectra showed two peaks at 262 nm ( $n$  to  $\pi^*$ ) and 313 nm ( $\pi$  to  $\pi^*$ ) transitions. Notably, compounds **19b** and **19c** showed peaks at 262 nm and 313 nm, 263 nm and

312 nm, respectively. The graph also revealed an isosbestic point at 291 nm, as illustrated in Fig. 11. Additionally, the spectra for compounds **19d**, **19e**, and **19f** showed absorption maxima at 262 nm for the  $n$  to  $\pi^*$  transition and 312 nm for the  $\pi$  to  $\pi^*$  transition, with the same isosbestic point at 291 nm. Similarly, compounds **19g**, **19h** and **19i** displayed  $\lambda_{\text{max}}$  at 262 nm, 262 nm and 263 nm for the  $n$  to  $\pi^*$  transition and 313 nm, 312 nm and 313 nm for the  $\pi$  to  $\pi^*$  transition, respectively. It was observed that increasing the chain length at the  $R_2$  position in the chromene moiety resulted in a shift from hypochromic to hyperchromic in the intensity of the UV-visible spectra.

On the other hand, a blue shift to red shift (from 312 to 321 nm) was observed in compound **19j** when a methyl group was introduced at the  $R_1$  position of the chromene framework, accompanied by a gradual decrease in optical density (OD). Similarly, a slight change in absorption maxima was noted in compound **19k** compared to **19j**. In a similar fashion, the absorption maxima and optical density of compounds **19l**, **19m**, and **19n** were compared, showing peaks at 265 nm, 265 nm, and 266 nm for the  $n$  to  $\pi^*$  transition, and 320 nm, 321 nm, and 320 nm for the  $\pi$  to  $\pi^*$  transition, respectively. An isosbestic point appeared at 297 nm for compounds **19l**, **19m**, and **19n**. Furthermore, the UV-visible spectra of three different synthesized molecules (**19o**, **19p**, and **19q**), where a phenyl group was

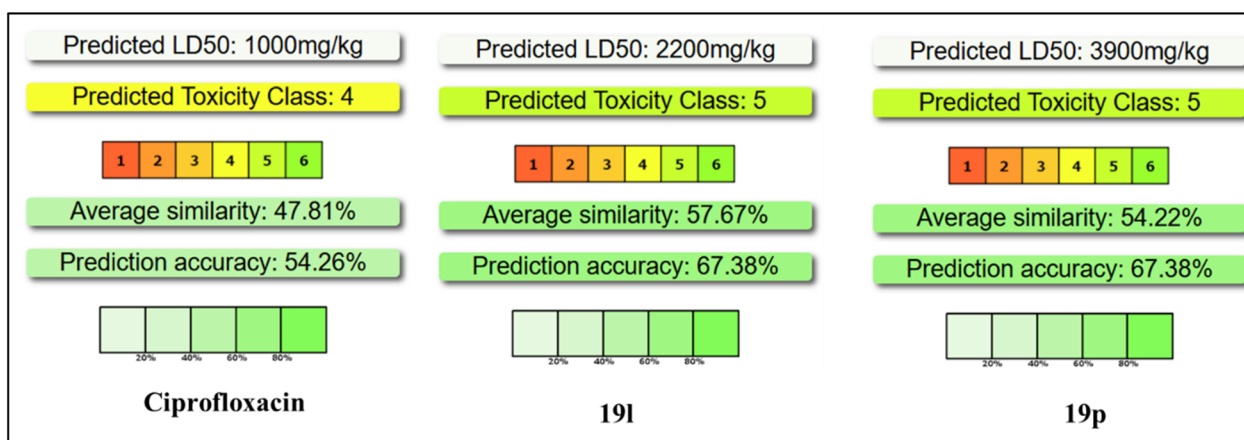


Fig. 10 Theoretical toxicity results of ciprofloxacin and synthesized compounds **19l** and **19p** calculated using ProTox 3.0.



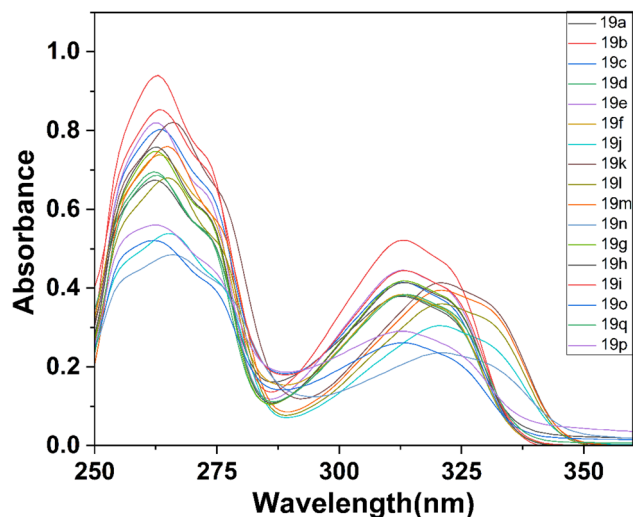


Fig. 11 UV-visible spectra of compounds 19(a–q) in DMSO medium.

introduced at the  $R_4$  position, showed a slight decrease in intensity compared to compounds 19a, 19b and 19c. The overall UV-visible spectra are shown in Fig. 11.

#### 4.2. Fluorescence studies

To examine the fluorescence properties of the series of tetrahydrochromeno[3,4-*e*]isoindole-1,3(2*H*,3*aH*)-dione derivatives 19(a–q), fluorescence experiments were conducted using fluorescence spectrometry Hitachi-7000 keeping the fluorescence slit width at 2.5 nm for each. A specific concentration (15  $\mu$ M) was maintained for all synthesized compounds during the assay. At the beginning of our experiment, compound 19a showed a wavelength of 352 nm with an optical density of 6151. Compound 19b, which has a methyl group introduced at the  $R_3$  position of the 4-styrylaromatic ring, showed a recorded wavelength of 352 nm with a slight increase in OD to 8421. Similarly, compounds 19c, 19d, 19e, 19f, 19g, 19h, and 19i showed the

same  $\lambda_{\text{max}}$  (352 nm) value with a gradual increase in OD values ranging from 8053 to 9784. It is noted that the increase in the chain length at the  $R_2$  position in the chromene analogue led to a corresponding increase in the optical density value (6151–9784).

However, a blue shift to red shift (from 352 to 363 nm) was observed for compound 19j, which exhibited notably strong fluorescence intensity amongst all the synthesized derivatives. Also, the compounds 19k, 19l and 19n have the same wave number at 361 nm with OD values of 6615, 6516 and 5127, respectively. Consequently, compounds 19o, 19p, and 19q displayed similar  $\lambda_{\text{max}}$  at 353 nm, comparable to compounds 19a, 19b, and 19c. Finally, it was observed that all the synthesized derivatives demonstrated good fluorescent activity, as illustrated in Fig. 12.

## 5. Conclusion

In this study, a class of fused tetrahydrochromeno[3,4-*e*]isoindole-1,3(2*H*,3*aH*)-dione derivatives were synthesized with good to excellent yields without the need for column chromatography. The reaction was carried out under mild conditions, yielding compounds with good binding affinities, potent antibacterial activity, and favorable photophysical properties, making this method highly efficient and practical. The *in vitro* results revealed that compounds 19l and 19p showed the most potent antibacterial activity against the tested pathogenic strains. Also, these results have been explained by the binding energy parameters determined from molecular docking studies, which showed that the selected compounds can bind with bacterial DNA gyrase more efficiently, similar to the antibiotic ciprofloxacin. Interestingly, the ADMET parameter prediction indicated that the majority of the synthesized conjugates have an acceptable pharmacokinetic profile with a nontoxic characteristic. Moreover, the photophysical properties are suitable for *in vivo* high-resolution microscope imaging. We propose that in the future, this strategy can be applied to medicinal chemistry for the synthesis of natural products with pharmacological activity and drug-containing structure of tetrahydrochromenoisoindole dione derivatives.

## 6. Experimental section

The commercially available reactants and reagents required for this reaction were purchased from the standard supplier (Sigma-Aldrich, TCI) and were used without further purification. All the reactions were carried out in anhydrous conditions. The progress of each reaction was monitored by thin-layer chromatography (TLC) on silica gel 60 (F254) coated with aluminum plates. Visualization of spots on the TLC plate was accomplished with UV light (254 nm).  $^1\text{H}$  NMR spectra were recorded on a 400 MHz (100 MHz for  $^{13}\text{C}$  NMR) JEOL NMR spectrometer using  $\text{CDCl}_3$  as solvent. High-resolution mass spectra (HRMS) were recorded using a Bruker micro TOF-QII mass spectrometer at IISER-Berhampur. The chemical shift was calibrated to tetramethyl silane (TMS) as an internal reference. Chemical shifts ( $\delta$ ) are given in ppm and coupling

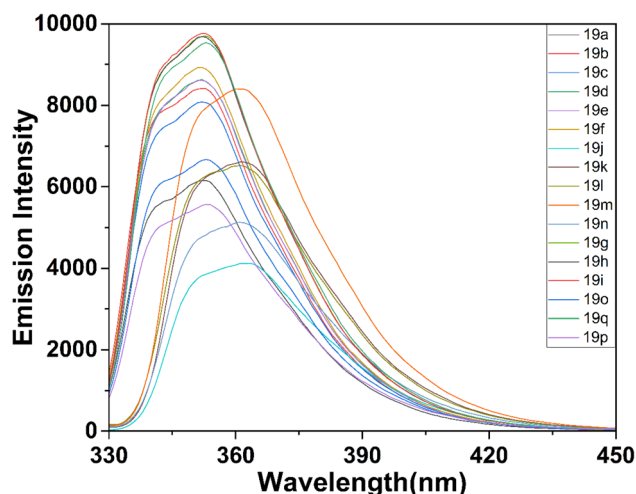


Fig. 12 Fluorescence spectra of compounds 19(a–q) in DMSO medium.



constants (*J*) in Hertz (Hz). The following abbreviations are used to indicate the signal multiplicity: s, singlet; d, doublet; t, triplet; q, quartet; m, multiplet. Melting points were determined using a SMP-10 digital apparatus and were uncorrected. The UV-visible and fluorescent spectra were taken in a Shimadzu single monochromator UV-2600 spectrophotometer and HITACHI F-7000 fluorescence spectrometer machine at Sambalpur University.

## 7. Experimental procedure

### 7.1. General experimental procedure for the preparation of substituted chroman-4-one 13(a-e)

In a 100 mL clean and dry round bottom (RB) flask, substituted *o*-hydroxyacetophenone (1.0 equiv.) **11(a-b)**, substituted ketone (3 equiv.) **12(a-c)** and pyrrolidine (0.5 equiv.) were taken. The mixture was stirred under a reflux medium for about 6–8 h. The reaction progress was monitored by TLC and was found to be completed after 6–8 h. After cooling to room temperature, the reaction mixture was quenched using water and extracted with ethyl acetate. The organic layer was washed with brine solution, dried over anhydrous Na<sub>2</sub>SO<sub>4</sub> and evaporated under reduced pressure. The crude product was purified by column chromatography using ethyl acetate/hexane to afford the pure compound **13(a-e)**. All compounds were characterized by NMR.

### 7.2. General experimental procedure for the synthesis of 4-bromo-2*H*-chromene derivatives 15(a-e)

Substituted chroman-4-one, (1.0 equiv.) **13(a-e)** and phosphorus tribromide (PBr<sub>3</sub>) **14** (3 equiv.) were taken in a clean and dry round bottom flask and stirred under reflux condition for 30–40 min. Set up by a trap using cotton and anhydrous calcium chloride. After completion, the reaction mixture was quenched using ice water and extracted with ethyl acetate. The organic layer was washed with brine, separated, dried over anhydrous Na<sub>2</sub>SO<sub>4</sub> and concentrated. The crude product was purified by column chromatography using ethyl acetate/hexane to furnish the pure compound **15(a-e)**. All compounds were characterized by NMR data.

### 7.3. General experimental procedure for the synthesis of 4-styryl-2*H*-chromene derivatives 17(a-n)

Substituted 4-bromo-2*H*-chromene, (1.0 equiv.) **15(a-e)**, substituted styrene (2.0 equiv.) **16(a-c)**, palladium(II) complex (0.1 equiv.), K<sub>2</sub>CO<sub>3</sub> (3.0 equiv.) and 1.5 mL of dry DMF were taken in the same vial and subjected to microwave irradiation at 120 °C, 100 W for about 20 min. The reaction was monitored by TLC and was found to be completed after 20 min. After completion, the reaction mixture was quenched using water and extracted with ethyl acetate. The organic layer was washed with brine, separated, dried over anhydrous Na<sub>2</sub>SO<sub>4</sub> and concentrated. The crude product was purified by flask column chromatography using ethyl acetate/hexane to afford the pure compound **17(a-n)**. It gives two isomer which is not separated.

### 7.4. General experimental procedure for the synthesis of tetrahydrochromeno[3,4-*e*]isoindole-1,3(2*H*,3*aH*)-dione derivatives 19(a-q)

Substituted 4-styryl-2*H*-chromene, (1.0 equiv.) **17(a-n)**, malimide (3.0 equiv.) **18(a-b)**, and 3 mL of dry toluene were taken in a sealed tube and stirred under reflux condition at 120 °C for 4 h. The reaction was monitored by TLC and was found to be completed after 4 h. Then, the reaction was cooled at room temperature, washed with hexane and filtered to afford a pure white solid compound **19(a-q)**. The compound was characterized by NMR and HRMS spectral data.

### 7.5. General experimental procedure for the synthesis of 11-(4-methoxyphenyl)-2-methyl-4,4-dipropylchromeno[3,4-*e*]isoindole-1,3(2*H*,4*H*)-dione (21)

11-(4-Methoxyphenyl)-2-methyl-4,4-dipropyl-3b,4,11,11a-tetrahydrochromeno[3,4-*e*]isoindole-1,3(2*H*,3*aH*)-dione (1.0 equiv.) **19i**, DDQ (2,3-dichloro-5,6-dicyano-1,4-benzoquinone) (1.5 equiv.) and 2 mL of dry toluene were taken in a clean and dry sealed tube and allowed to stir at 100 °C for 30 min. The progress of the reaction was monitored by TLC and after completion of the reaction, the pure compound **21** was obtained using column chromatography using ethyl acetate/hexane. After synthesis, the compound was characterized using <sup>1</sup>H NMR, <sup>13</sup>C NMR and HRMS spectroscopic techniques.

**7.5.1 2,4,4-Trimethyl-11-phenyl-3b,4,11,11a-tetrahydrochromeno[3,4-*e*]isoindole-1,3(2*H*,3*aH*)-dione (19a).** White solid (91% yield), M.P. = 258–260, <sup>1</sup>H NMR (400 MHz, CDCl<sub>3</sub>): δ (ppm) 7.44 (dd, *J*<sub>12</sub> = 1.6 Hz, *J*<sub>13</sub> = 8.0 Hz, 1H), 7.36–7.32 (m, 2H), 7.28–7.25 (m, 3H), 7.12–7.08 (m, 1H), 6.88–6.81 (m, 2H), 6.59–6.57 (m, 1H), 3.73–3.70 (m, 1H), 3.52–3.49 (m, 1H), 3.38–3.34 (m, 1H), 2.65 (s, 4H), 1.82 (s, 3H), 1.30 (s, 3H). <sup>13</sup>C NMR (100 MHz, CDCl<sub>3</sub>): δ (ppm) 175.7, 175.3, 152.7, 138.7, 133.2, 129.5, 128.8 (2C), 128.3 (2C), 127.3, 122.5, 121.1, 120.9 (2C), 119.0, 75.1, 48.1, 45.7, 42.8, 42.6, 29.1, 26.0, 24.8. HRMS (ESI) calculated for C<sub>24</sub>H<sub>24</sub>NO<sub>3</sub> [M + H]<sup>+</sup> 374.1756, found 374.1780.

**7.5.2 2,4,4-Trimethyl-11-(*p*-tolyl)-3b,4,11,11a-tetrahydrochromeno[3,4-*e*]isoindole-1,3(2*H*,3*aH*)-dione (19b).** White solid (94% yield), M.P. = 253–255, <sup>1</sup>H NMR (400 MHz, CDCl<sub>3</sub>): δ (ppm) 7.43 (dd, *J*<sub>12</sub> = 1.2 Hz, *J*<sub>13</sub> = 7.6 Hz, 1H), 7.19 (s, 1H), 7.14 (s, 3H), 7.11–7.07 (m, 1H), 6.87–6.80 (m, 2H), 6.56–6.54 (m, 1H), 3.70–3.67 (m, 1H), 3.51–3.47 (m, 1H), 3.35–3.31 (m, 1H), 2.65 (s, 4H), 2.31 (s, 3H), 1.81 (s, 3H), 1.30 (s, 3H). <sup>13</sup>C NMR (100 MHz, CDCl<sub>3</sub>): δ (ppm) 175.7, 175.4, 152.6, 136.8, 135.6, 133.0, 129.4, 129.1 (2C), 128.7 (2C), 122.5, 121.2, 121.1, 120.9, 118.9, 75.1, 48.2, 45.6, 42.6, 42.5, 29.1, 26.0, 24.7, 21.1. HRMS (ESI) calculated for C<sub>25</sub>H<sub>26</sub>NO<sub>3</sub> [M + H]<sup>+</sup> 388.1913, found 388.1903.

**7.5.3 11-(4-methoxyphenyl)-2,4,4-trimethyl-3b,4,11,11a-tetrahydrochromeno[3,4-*e*]isoindole-1,3(2*H*,3*aH*)-dione (19c).** White solid (92% yield), M.P. = 267–269, <sup>1</sup>H NMR (400 MHz, CDCl<sub>3</sub>): δ (ppm) 7.43 (dd, *J*<sub>12</sub> = 1.2 Hz, *J*<sub>13</sub> = 7.6 Hz, 1H), 7.19–7.17 (m, 2H), 7.17–7.16 (m, 1H), 7.11–7.07 (m, 1H), 6.88–6.80 (m, 3H), 6.53–6.51 (m, 1H), 3.76 (s, 3H), 3.69–3.66 (m, 1H), 3.50–3.47 (m, 1H), 3.32–3.29 (m, 1H), 2.65 (s, 4H), 2.09 (s, 3H), 1.81 (s, 3H), 1.30 (s, 3H). <sup>13</sup>C NMR (100 MHz, CDCl<sub>3</sub>): δ (ppm) 175.8, 175.4, 158.7, 152.6, 132.9, 130.6, 129.8 (2C), 129.4, 122.5, 121.4, 121.0,



120.9, 118.9, 113.7 (2C), 75.1, 55.2, 48.1, 45.6, 42.5, 42.1, 29.1, 25.9, 24.7. HRMS (ESI) calculated for  $C_{25}H_{26}NO_4$   $[M + H]^+$  404.1862, found 404.1877.

**7.5.4 4,4-Diethyl-2-methyl-11-phenyl-3*b*,4,11,11*a*-tetrahydrochromeno[3,4-*e*]isoindole-1,3(2*H*,3*aH*)-dione (19d).** White solid (88% yield), M.P. = 249–251,  $^1H$  NMR (400 MHz,  $CDCl_3$ ):  $\delta$  (ppm) 7.50 (dd,  $J_{12} = 1.2$  Hz,  $J_{13} = 8.0$  Hz, 1H), 7.43–7.40 (m, 2H), 7.35–7.33 (m, 3H), 7.19–7.15 (m, 1H), 6.95 (dd,  $J_{12} = 0.8$  Hz,  $J_{13} = 8.4$  Hz, 1H), 6.91–6.87 (m, 1H), 6.64–6.62 (m, 1H), 3.80–3.77 (m, 1H), 3.56–3.53 (m, 1H), 3.45–3.41 (m, 1H), 2.73 (s, 4H), 2.43–2.28 (m, 2H), 1.81–1.75 (m, 1H), 1.52–1.47 (m, 1H), 1.08 (t,  $J = 7.6$  Hz, 3H), 0.84 (t,  $J = 7.2$  Hz, 3H).  $^{13}C$  NMR (100 MHz,  $CDCl_3$ ):  $\delta$  (ppm) 175.6, 175.4, 152.1, 138.6, 133.4, 129.5, 128.8 (2C), 128.3 (2C), 127.2, 122.4, 121.4, 120.9, 120.8, 118.9, 79.3, 48.4, 43.2, 42.8, 42.3, 27.3, 25.5, 24.8, 8.3, 7.5. HRMS (ESI) calculated for  $C_{26}H_{28}NO_3$   $[M + H]^+$  402.2069, found 402.2081.

**7.5.5 4,4-Diethyl-2-methyl-11-(*p*-tolyl)-3*b*,4,11,11*a*-tetrahydrochromeno[3,4-*e*]isoindole-1,3(2*H*,3*aH*)-dione (19e).** White solid (91% yield), M.P. = 245–247,  $^1H$  NMR (400 MHz,  $CDCl_3$ ):  $\delta$  (ppm) 7.49 (dd,  $J_{12} = 1.2$  Hz,  $J_{13} = 7.6$  Hz, 1H), 7.22 (s, 4H), 7.19–7.15 (m, 1H), 6.95 (dd,  $J_{12} = 1.2$  Hz,  $J_{13} = 8.4$  Hz, 1H), 6.90–6.86 (m, 1H), 6.62–6.60 (m, 1H), 3.77–3.74 (m, 1H), 3.55–3.51 (m, 1H), 3.42–3.38 (m, 1H), 2.73 (s, 3H), 2.72–2.71 (m, 1H), 2.38 (s, 3H), 2.36–2.27 (m, 2H), 1.80–1.75 (m, 1H), 1.54–1.46 (m, 1H), 1.08 (t,  $J = 7.6$  Hz, 3H), 0.83 (t,  $J = 7.6$  Hz, 3H).  $^{13}C$  NMR (100 MHz,  $CDCl_3$ ):  $\delta$  (ppm) 175.7, 175.5, 152.1, 136.8, 135.5, 134.2, 133.3, 129.4, 129.1 (2C), 128.6 (2C), 122.4, 121.2, 120.9, 118.9, 79.3, 48.5, 43.2, 42.5, 42.4, 27.3, 25.5, 24.8, 21.1, 8.3, 7.5. HRMS (ESI) calculated for  $C_{27}H_{30}NO_3$   $[M + H]^+$  416.2226, found 416.2214.

**7.5.6 4,4-Diethyl-11-(4-methoxyphenyl)-2-methyl-3*b*,4,11,11*a*-tetrahydrochromeno[3,4-*e*]isoindole-1,3(2*H*,3*aH*)-dione (19f).** White solid (89% yield), M.P. = 254–256,  $^1H$  NMR (400 MHz,  $CDCl_3$ ):  $\delta$  (ppm) 7.49 (dd,  $J_{12} = 0.8$  Hz,  $J_{13} = 8.0$  Hz, 1H), 7.25–7.23 (m, 2H), 7.18–7.14 (m, 1H), 6.95–6.93 (m, 3H), 6.90–6.86 (m, 1H), 6.59–6.57 (m, 1H), 3.83 (s, 3H), 3.76–3.73 (m, 1H), 3.54–3.50 (m, 1H), 3.39–3.35 (m, 1H), 2.73 (s, 4H), 2.42–2.27 (m, 2H), 1.82–1.73 (m, 1H), 1.54–1.45 (m, 1H), 1.08 (t,  $J = 7.6$  Hz, 3H), 0.83 (t,  $J = 7.6$  Hz, 3H).  $^{13}C$  NMR (100 MHz,  $CDCl_3$ ):  $\delta$  (ppm) 175.8, 175.4, 158.7, 152.1, 133.2, 130.6, 129.8 (2C), 129.4, 122.3, 121.4, 121.3, 120.9, 118.9, 113.7 (2C), 79.3, 55.2, 48.4, 43.2, 42.3, 42.2, 27.3, 25.5, 24.8, 8.2, 7.5. HRMS (ESI) calculated for  $C_{27}H_{30}NO_4$   $[M + H]^+$  432.2175, found 432.2183.

**7.5.7 2-Methyl-11-phenyl-4,4-dipropyl-3*b*,4,11,11*a*-tetrahydrochromeno[3,4-*e*]isoindole-1,3(2*H*,3*aH*)-dione (19g).** White solid (83% yield), M.P. = 260–262,  $^1H$  NMR (400 MHz,  $CDCl_3$ ):  $\delta$  (ppm) 7.43 (dd,  $J_{12} = 1.6$  Hz,  $J_{13} = 8.0$  Hz, 1H), 7.36–7.32 (m, 2H), 7.28–7.25 (m, 3H), 7.11–7.07 (m, 1H), 6.87–6.79 (m, 2H), 6.56–6.54 (m, 1H), 3.71–3.68 (m, 1H), 3.44–3.41 (m, 1H), 3.36–3.32 (m, 1H), 2.66 (s, 3H), 2.64 (s, 1H), 2.24–2.15 (m, 2H), 1.62–1.52 (m, 2H), 1.37–1.22 (m, 4H), 1.00 (t,  $J = 7.2$  Hz, 3H), 0.68 (t,  $J = 7.6$  Hz, 3H).  $^{13}C$  NMR (100 MHz,  $CDCl_3$ ):  $\delta$  (ppm) 175.6, 175.3, 152.1, 138.6, 133.5, 129.4, 128.8 (2C), 128.3 (2C), 127.2, 122.3, 121.3, 120.9, 120.8, 118.9, 78.8, 48.4, 43.7, 42.8, 42.4, 37.9, 36.1, 24.8, 17.1, 16.6, 14.6, 14.2. HRMS (ESI) calculated for  $C_{28}H_{32}NO_3$   $[M + H]^+$  430.2382, found 430.2392.

**7.5.8 2-Methyl-4,4-dipropyl-11-(*p*-tolyl)-3*b*,4,11,11*a*-tetrahydrochromeno[3,4-*e*]isoindole-1,3(2*H*,3*aH*)-dione (19h).** White solid (89% yield), M.P. = 257–259,  $^1H$  NMR (400 MHz,  $CDCl_3$ ):  $\delta$  (ppm) 7.42 (dd,  $J_{12} = 0.8$  Hz,  $J_{13} = 7.6$  Hz, 1H), 7.14 (s, 4H), 7.11–7.07 (m, 1H), 6.86–6.79 (m, 2H), 6.54–6.52 (m, 1H), 3.68–3.65 (m, 1H), 3.43–3.40 (m, 1H), 3.33–3.29 (m, 1H), 2.66 (s, 3H), 2.63 (s, 1H), 2.31 (s, 3H), 2.22–2.16 (m, 2H), 1.63–1.53 (m, 2H), 1.35–1.25 (m, 4H), 1.00 (t,  $J = 7.2$  Hz, 3H), 0.68 (t,  $J = 7.2$  Hz, 3H).  $^{13}C$  NMR (100 MHz,  $CDCl_3$ ):  $\delta$  (ppm) 175.7, 175.4, 152.0, 136.8, 135.6, 133.4, 129.4, 129.1 (2C), 128.6 (2C), 122.3, 121.3, 121.1, 120.8, 118.9, 78.8, 48.5, 43.6, 42.5, 42.4, 37.9, 36.1, 24.8, 21.1, 17.2, 16.6, 14.6, 14.2. HRMS (ESI) calculated for  $C_{29}H_{34}NO_3$   $[M + H]^+$  444.2539, found 444.2552.

**7.5.9 11-(4-methoxyphenyl)-2-methyl-4,4-dipropyl-3*b*,4,11,11*a*-tetrahydrochromeno[3,4-*e*]isoindole-1,3(2*H*,3*aH*)-dione (19i).** White solid (85% yield), M.P. = 261–263,  $^1H$  NMR (400 MHz,  $CDCl_3$ ):  $\delta$  (ppm) 7.49 (dd,  $J_{12} = 1.2$  Hz,  $J_{13} = 7.6$  Hz, 1H), 7.25–7.23 (m, 2H), 7.18–7.13 (m, 1H), 6.95–6.85 (m, 4H), 6.58–6.56 (m, 1H), 3.83 (s, 3H), 3.74–3.71 (m, 1H), 3.48–3.46 (m, 1H), 3.38–3.34 (m, 1H), 2.73 (s, 3H), 2.70 (s, 1H), 2.29–2.24 (m, 2H), 1.70–1.61 (m, 3H), 1.39–1.33 (m, 3H), 1.07 (t,  $J = 7.2$  Hz, 3H), 0.76 (t,  $J = 7.2$  Hz, 3H).  $^{13}C$  NMR (100 MHz,  $CDCl_3$ ):  $\delta$  (ppm) 175.7, 175.4, 158.7, 152.1, 133.3, 130.6, 129.8 (2C), 129.4, 122.3, 121.3, 121.2, 120.8, 118.9, 113.7 (2C), 78.8, 55.2, 48.4, 43.6, 42.4, 42.2, 37.9, 36.1, 24.8, 17.1, 16.6, 14.6, 14.2. HRMS (ESI) calculated for  $C_{29}H_{34}NO_4$   $[M + H]^+$  460.2488, found 460.2479.

**7.5.10 2,4,4,8-Tetramethyl-11-phenyl-3*b*,4,11,11*a*-tetrahydrochromeno[3,4-*e*]isoindole 1,3(2*H*,3*aH*)-dione (19j).** White solid (88% yield), M.P. = 246–248,  $^1H$  NMR (400 MHz,  $CDCl_3$ ):  $\delta$  (ppm) 7.36–7.32 (m, 2H), 7.28–7.24 (m, 4H), 6.91 (dd,  $J_{12} = 1.2$  Hz,  $J_{13} = 8.0$  Hz, 1H), 6.78–6.75 (m, 1H), 6.56–6.54 (m, 1H), 3.72–3.69 (m, 1H), 3.51–3.48 (m, 1H), 3.37–3.34 (m, 1H), 2.65 (s, 3H), 2.64 (s, 1H), 2.20 (s, 3H), 1.80 (s, 3H), 1.28 (s, 3H).  $^{13}C$  NMR (100 MHz,  $CDCl_3$ ):  $\delta$  (ppm) 175.7, 175.3, 150.5, 138.7, 133.3, 130.3, 130.2, 128.8 (2C), 128.3 (2C), 127.2, 122.7, 120.6, 120.5, 118.7, 74.9, 48.1, 45.6, 42.8, 42.6, 29.1, 26.0, 24.8, 20.8. HRMS (ESI) calculated for  $C_{25}H_{26}NO_3$   $[M + H]^+$  388.1913, found 388.1903.

**7.5.11 11-(4-Methoxyphenyl)-2,4,4,8-tetramethyl-3*b*,4,11,11*a*-tetrahydrochromeno[3,4-*e*]isoindole-1,3(2*H*,3*aH*)-dione (19k).** White solid (90% yield), M.P. = 247–249,  $^1H$  NMR (400 MHz,  $CDCl_3$ ):  $\delta$  (ppm) 7.22 (d,  $J = 1.6$  Hz, 1H), 7.19–7.16 (m, 3H), 6.90 (dd,  $J_{12} = 1.6$  Hz,  $J_{13} = 8.0$  Hz, 1H), 6.88–6.85 (m, 2H), 6.76 (d,  $J = 8.4$  Hz, 1H), 6.50–6.49 (m, 1H), 3.76 (s, 3H), 3.69–3.64 (m, 1H), 3.48–3.45 (m, 1H), 3.31–3.28 (m, 1H), 2.65 (s, 3H), 2.62 (s, 1H), 2.19 (s, 3H), 1.79 (s, 3H), 1.28 (s, 3H).  $^{13}C$  NMR (100 MHz,  $CDCl_3$ ):  $\delta$  (ppm) 175.9, 175.4, 158.7, 150.5, 133.1, 130.7, 130.3, 130.1, 129.8 (2C), 122.7, 121.1, 120.5, 118.7, 113.7 (2C), 74.9, 55.2, 48.2, 45.5, 42.6, 42.1, 29.0, 25.9, 24.8, 20.7. HRMS (ESI) calculated for  $C_{26}H_{28}NO_4$   $[M + H]^+$  418.2018, found 418.2027.

**7.5.12 4,4-Diethyl-2,8-dimethyl-11-phenyl-3*b*,4,11,11*a*-tetrahydrochromeno[3,4-*e*]isoindole-1,3(2*H*,3*aH*)-dione (19l).** White solid (84% yield), M.P. = 250–252,  $^1H$  NMR (400 MHz,  $CDCl_3$ ):  $\delta$  (ppm) 7.44–7.40 (m, 2H), 7.36–7.32 (m, 3H), 7.31–7.30 (m, 1H), 6.98 (dd,  $J_{12} = 1.6$  Hz,  $J_{13} = 8.0$  Hz, 1H), 6.87–6.85 (m, 1H), 6.62–6.60 (m, 1H), 3.80–3.77 (m, 1H), 3.55–3.52 (m, 1H),



3.45–3.41 (m, 1H), 2.74 (s, 3H), 2.69 (s, 1H), 2.42–2.29 (m, 2H), 2.27 (s, 3H), 1.82–1.74 (m, 1H), 1.52–1.45 (m, 1H), 1.08 (t,  $J = 7.6$  Hz, 3H), 0.83 (t,  $J = 7.2$  Hz, 3H).  $^{13}\text{C}$  NMR (100 MHz,  $\text{CDCl}_3$ ):  $\delta$  (ppm) 175.7, 175.4, 149.9, 138.7, 133.5, 130.3, 130.0, 128.8 (2C), 128.3 (2C), 127.2, 122.6, 121.0, 120.6, 118.7, 79.1, 48.4, 43.2, 42.8, 42.4, 27.2, 25.5, 24.9, 20.8, 8.3, 7.5. HRMS (ESI) calculated for  $\text{C}_{27}\text{H}_{30}\text{NO}_3$   $[\text{M} + \text{H}]^+$  416.2226, found 416.2238.

**7.5.13 4,4-Diethyl-2,8-dimethyl-11-(*p*-tolyl)-3*b*,4,11,11*a*-tetrahydrochromeno[3,4-*e*]isoindole-1,3(2*H*,3*aH*)-dione (19m).** White solid (89% yield), M.P. = 251–253,  $^1\text{H}$  NMR (400 MHz,  $\text{CDCl}_3$ ):  $\delta$  (ppm) 7.29 (d,  $J = 1.6$  Hz, 1H), 7.23 (s, 4H), 6.97 (dd,  $J_{12} = 1.6$  Hz,  $J_{13} = 8.4$  Hz, 1H), 6.86–6.84 (m, 1H), 6.59–6.57 (m, 1H), 3.76–3.73 (m, 1H), 3.53–3.50 (m, 1H), 3.41–3.37 (m, 1H), 2.73 (s, 3H), 2.68 (s, 1H), 2.38 (s, 3H), 2.35–2.29 (m, 2H), 2.27 (s, 3H), 1.79–1.74 (m, 1H), 1.50–1.44 (m, 1H), 1.07 (t,  $J = 8.0$  Hz, 3H), 0.82 (t,  $J = 7.6$  Hz, 3H).  $^{13}\text{C}$  NMR (100 MHz,  $\text{CDCl}_3$ ):  $\delta$  (ppm) 175.8, 175.5, 149.9, 136.8, 135.6, 133.4, 130.3, 130.0, 129.1 (2C), 128.6 (2C), 122.6, 121.1, 120.9, 118.7, 79.1, 48.5, 43.2, 42.5, 42.4, 27.2, 25.5, 24.8, 21.1, 20.8, 8.3, 7.5. HRMS (ESI) calculated for  $\text{C}_{28}\text{H}_{32}\text{NO}_3$   $[\text{M} + \text{H}]^+$  430.2382, found 430.2387.

**7.5.14 4,4-Diethyl-11-(4-methoxyphenyl)-2,8-dimethyl-3*b*,4,11,11*a*-tetrahydrochromeno[3,4-*e*]isoindole-1,3(2*H*,3*aH*)-dione (19n).** White solid (86% yield), M.P. = 258–260,  $^1\text{H}$  NMR (400 MHz,  $\text{CDCl}_3$ ):  $\delta$  (ppm) 7.29 (d,  $J = 1.6$  Hz, 1H), 7.27–7.24 (m, 1H), 6.99–6.94 (m, 3H), 6.86–6.84 (m, 1H), 6.56–6.55 (m, 1H), 3.84 (s, 3H), 3.75–3.72 (m, 1H), 3.52–3.50 (m, 1H), 3.39–3.35 (m, 1H), 2.74 (s, 3H), 2.68 (s, 1H), 2.41–2.29 (m, 2H), 2.27 (s, 3H), 2.17 (s, 3H), 1.79–1.74 (m, 1H), 1.50–1.44 (m, 1H), 1.07 (t,  $J = 7.6$  Hz, 3H), 0.82 (t,  $J = 7.2$  Hz, 3H).  $^{13}\text{C}$  NMR (100 MHz,  $\text{CDCl}_3$ ):  $\delta$  (ppm) 175.8, 175.5, 158.6, 149.9, 133.4, 130.7, 130.3, 130.0, 129.8 (2C), 122.6, 121.1, 121.0, 118.7, 113.7 (2C), 79.1, 55.2, 48.4, 43.1, 42.4, 42.1, 27.2, 25.5, 24.9, 20.8, 8.3, 7.5. HRMS (ESI) calculated for  $\text{C}_{28}\text{H}_{32}\text{NO}_4$   $[\text{M} + \text{H}]^+$  446.2331, found 446.2325.

**7.5.15 4,4-Dimethyl-2,11-diphenyl-3*b*,4,11,11*a*-tetrahydrochromeno[3,4-*e*]isoindole-1,3(2*H*,3*aH*)-dione (19o).** White solid (76% yield), M.P. = 263–265,  $^1\text{H}$  NMR (400 MHz,  $\text{CDCl}_3$ ):  $\delta$  (ppm) 7.56 (dd,  $J_{12} = 1.2$  Hz,  $J_{13} = 7.6$  Hz, 1H), 7.41–7.36 (m, 4H), 7.35–7.27 (m, 2H), 7.25–7.18 (m, 3H), 6.95–6.89 (m, 2H), 6.84–6.82 (m, 2H), 6.81–6.76 (m, 1H), 3.91–3.89 (m, 1H), 3.75–3.72 (m, 1H), 3.63–3.59 (m, 1H), 2.87–2.84 (m, 1H), 1.92 (s, 3H), 1.44 (s, 3H).  $^{13}\text{C}$  NMR (100 MHz,  $\text{CDCl}_3$ ):  $\delta$  (ppm) 174.7, 174.5, 152.5, 138.5, 133.8, 131.5, 129.6, 128.9 (2C), 128.7 (2C), 128.4 (2C), 128.2, 127.3, 126.2, 122.5, 121.1, 120.9, 120.6, 118.9, 75.2, 48.4, 45.8, 42.8, 42.3, 28.9, 25.7. HRMS (ESI) calculated for  $\text{C}_{29}\text{H}_{26}\text{NO}_3$   $[\text{M} + \text{H}]^+$  436.1913, found 436.1926.

**7.5.16 4,4-Dimethyl-2-phenyl-11-(*p*-tolyl)-3*b*,4,11,11*a*-tetrahydrochromeno[3,4-*e*]isoindole-1,3(2*H*,3*aH*)-dione (19p).** White solid (79% yield), M.P. = 260–262,  $^1\text{H}$  NMR (400 MHz,  $\text{CDCl}_3$ ):  $\delta$  (ppm) 7.49 (dd,  $J_{12} = 2.0$  Hz,  $J_{13} = 7.6$  Hz, 1H), 7.22–7.20 (m, 3H), 7.18–7.08 (m, 5H), 6.87–6.81 (m, 2H), 6.76–6.74 (m, 2H), 6.69–6.67 (m, 1H), 3.82–3.79 (m, 1H), 3.66–3.63 (m, 1H), 3.52–3.48 (m, 1H), 2.79–2.78 (m, 1H), 2.28 (s, 3H), 1.84 (s, 3H), 1.36 (s, 3H).  $^{13}\text{C}$  NMR (100 MHz,  $\text{CDCl}_3$ ):  $\delta$  (ppm) 174.8, 174.6, 152.5, 136.9, 135.4, 132.7, 131.6, 129.5, 129.1 (2C), 128.8 (2C), 128.7 (2C), 128.1, 126.2 (2C), 122.5, 121.2, 121.1, 120.6, 118.9, 75.3, 48.5, 45.8, 42.5, 42.3, 28.9, 25.6, 21.1. HRMS (ESI) calculated for  $\text{C}_{30}\text{H}_{28}\text{NO}_3$   $[\text{M} + \text{H}]^+$  450.2069, found 450.2048.

**7.5.17 4,4-Diethyl-2,11-diphenyl-3*b*,4,11,11*a*-tetrahydrochromeno[3,4-*e*]isoindole-1,3(2*H*,3*aH*)-dione (19q).** White solid (73% yield), M.P. = 264–266,  $^1\text{H}$  NMR (400 MHz,  $\text{CDCl}_3$ ):  $\delta$  (ppm) 7.55 (dd,  $J_{12} = 1.2$  Hz,  $J_{13} = 7.6$  Hz, 1H), 7.41–7.40 (m, 4H), 7.34–7.30 (m, 1H), 7.26–7.15 (m, 4H), 6.96–6.94 (m, 1H), 6.91–6.83 (m, 3H), 6.78–6.76 (m, 1H), 3.91–3.88 (m, 1H), 3.70–3.67 (m, 1H), 3.62–3.58 (m, 1H), 2.84–2.83 (m, 1H), 2.49–2.44 (m, 1H), 2.34–2.29 (m, 1H), 1.87–1.81 (m, 1H), 1.58–1.52 (m, 1H), 1.10 (t,  $J = 7.6$  Hz, 3H), 0.86 (t,  $J = 7.6$  Hz, 3H).  $^{13}\text{C}$  NMR (100 MHz,  $\text{CDCl}_3$ ):  $\delta$  (ppm) 174.6, 174.5, 151.9, 138.5, 133.2, 131.6, 129.5, 128.8 (2C), 128.7 (2C), 128.4 (2C), 128.1, 127.2, 126.1 (2C), 122.3, 121.1, 120.9 (2C), 118.9, 79.3, 48.8, 43.3, 42.8, 42.1, 27.2, 25.3, 8.2, 7.5. HRMS (ESI) calculated for  $\text{C}_{31}\text{H}_{30}\text{NO}_3$   $[\text{M} + \text{H}]^+$  464.2226, found 464.2223.

**7.5.18 11-(4-Methoxyphenyl)-2-methyl-4,4-dipropylchromeno[3,4-*e*]isoindole-1,3(2*H*,4*H*)-dione (21).** Light green liquid (78% yield),  $^1\text{H}$  NMR (400 MHz,  $\text{CDCl}_3$ ):  $\delta$  (ppm) 7.87 (s, 1H), 7.64 (dd,  $J_{12} = 1.6$  Hz,  $J_{13} = 8.0$  Hz, 1H), 7.54–7.48 (m, 2H), 7.30–7.25 (m, 1H), 7.02–6.91 (m, 4H), 3.88 (s, 3H), 3.12 (s, 3H), 2.72–2.64 (m, 2H), 2.05–1.97 (m, 2H), 1.53–1.43 (m, 2H), 1.23–1.16 (m, 2H), 0.85 (t,  $J = 7.6$  Hz, 3H).  $^{13}\text{C}$  NMR (100 MHz,  $\text{CDCl}_3$ ):  $\delta$  (ppm) 167.5, 167.2, 159.9, 154.4, 139.7, 136.5, 136.4, 131.4, 130.6 (2C), 128.9, 128.8, 128.7, 127.5, 123.7, 121.2, 119.1117.6, 113.4 (2C), 84.5, 55.3, 41.2 (2C), 24.0, 17.5 (2C), 14.4 (2C). HRMS (ESI) calculated for  $\text{C}_{29}\text{H}_{30}\text{NO}_4$   $[\text{M} + \text{H}]^+$  456.2175, found 456.2165.

## 8. Method of crystal growth

Compound **19i** was first dissolved in a minimal amount of ethyl acetate, followed by the addition of drops of hexane. This solution was then placed in a sample vial and stored in a dark area for 4 to 5 weeks to enable gradual evaporation. After 5 weeks, white needle-like crystals of compound **19i** were formed.

## 9. Molecular docking studies of compound **19(a–q)** against bacterial DNA gyrase of *E. coli* and *S. aureus*

All the synthesized derivatives **19(a–q)** were carefully drawn with proper stereochemistry and the 2D structures were converted to optimized 3D structures. Molecular docking studies were conducted using Autodock Tools version 4.2.0. The host proteins, including the bacterial DNA gyrase inhibitors for Gram-negative bacterial strain *E. coli* (PDB ID: 3 G7E) and Gram-positive bacterial strain *S. aureus* (PDB ID: 3 G7B), were downloaded and retrieved from the RCSB Protein Data Bank (<https://www.rcsb.org/>). Before docking the complex, water molecules and other hetero-atoms were removed from these host protein structures using PyMOL (<https://www.pymol.org/>).<sup>53,54</sup> Also, polar hydrogen bonds were added, and a grid box was set to  $60 \times 60 \times 60$  for the xyz axes (covering ligand binding pocket). 0.375 Å is the grid space for 100 genetic algorithm runs.<sup>2,55</sup> The two programs, 'autodock' and 'autogrid', were used to determine the binding affinity scores for the host-guest interaction. The 2D structures of ligand-receptor





interactions were visualized using PyMOL and BIOVIA Discovery Studio v 2017.

## 10. Antibacterial evaluation of compound 19(a–q) against bacterial DNA gyrase of *E. coli* and *S. aureus*

The *in vitro* antibacterial activity of all the synthesized molecules was tested using the agar-well diffusion method against *E. coli* (MTCC614) and *S. aureus* (MTCC7443) bacterial strains. Ciprofloxacin served as the standard antibiotic. Initially, the compounds were dissolved in DMSO and tested on Mueller–Hinton agar plates to assess the zones of inhibition (ZI). For the minimum inhibitory concentration (MIC) assay, the compounds were prepared at various concentrations (6.25, 12.5, 25, 50 and 100  $\mu\text{g mL}^{-1}$  and 200  $\mu\text{g mL}^{-1}$ ) and tested in a 96-well plate format to evaluate their bacterial inhibitory properties.

## 11. Physicochemical, pharmacokinetic and ADME studies

The ADME and pharmacokinetic properties of all the synthesized compounds were studied on the free online server Swiss ADME (<https://www.swissadme.ch/>). Initially, chemical structures were drawn on Marvin to generate SMILE and inserted directly on the webpage to initiate the prediction process.<sup>56–58</sup> The toxicity evaluation of the synthesized compounds 19(a–q) was determined using ProTox II free software.

## 12. Photophysical study

The photophysical (UV-visible and fluorescence) studies were performed for all the synthesized compounds using the Shimadzu single monochromator UV-2600 spectrophotometer and HITACHI F-7000 fluorescence spectrometer. Initially, the compounds were dissolved in DMSO at a uniform concentration (15  $\mu\text{M}$ ), and the spectra were recorded.<sup>59</sup>

## Data availability

The data supporting this article have been included as part of the ESI.†

## Author contributions

Sonali Priyadarshini Parida: conceptualization, investigation, methodology, formal analysis, data correction, writing-review & editing; Seetaram Mohapatra: supervision, resources, funding acquisition, editing; Suhasini Mohapatra: writing original draft, conceptualization, writing-review & editing; Tankadhar Behera: UV-visible & fluorescent study; Sabita Nayak: conceptualization, validation, supervision, funding acquisition, editing; software, resources; Chita Ranjan Sahoo: software, antibacterial studies.

## Conflicts of interest

The authors declare that they have no known competing financial interests or personal relationships that could have appeared to influence the work reported in this paper.

## Acknowledgements

The author, Seetaram Mohapatra, expresses gratitude to the Department of Science and Technology (DST), Odisha (ST-SCST-MISC-0011-2023, Bhubaneswar, 25-05-2023). He also acknowledges the Centre of Excellence in Environment and Public Health, Department of Higher Education, Government of Odisha (Grant no 26913/HED/HE-PTC-WB-02-17 OHEPEE). Author Sabita Nayak extends thanks to Mukhyamantri Research Innovation (MRI) for Extramural Research Grant-2024(24 EM/CH/35). The author, Sonali Priyadarshini Parida, also acknowledges DST, Odisha program (2692/ST, Bhubaneswar, 16-7-2020) for providing the financial support as a project assistant. Author Suhasini Mohapatra acknowledges the financial support from SERB-SURE, New Delhi (Ref. SUR/2022/000257). Additionally, the author is thankful to DST-FIST, New Delhi (SR/FST/CSI-243/2012) for the NMR facility.

## References

- 1 A. F. Al-burgus, O. T. Ali and O. Y. Al-abbasy, *Chim. Techno Acta*, 2024, **11**, 202411308.
- 2 C. R. Sahoo, S. K. Paidasetty, S. Sarathbabu, B. Dehury, N. S. Kumar and R. N. Padhy, *J. Biomol. Struct. Dyn.*, 2022, **40**, 11653–11663.
- 3 A. C. Singer, H. Shaw, V. Rhodes and A. Hart, *Front. Microbiol.*, 2016, **7**, 1728.
- 4 B. M. Marshall and S. B. Levy, *Clin. Microbiol. Rev.*, 2011, **24**, 718–733.
- 5 M. E. Faydy, L. Lakhrissi, N. Dahaieh, K. Ounine, B. Tuzun, N. Chahboun, A. Boshala, A. AlObaid, I. Warad, B. Lakhrissi and A. Zarrouk, *ACS Omega*, 2024, **9**, 25395–25409.
- 6 M. F. A. Mohamed, A. M. Soliman, O. Alshazly, A. Nafady and R. A. Soomro, *Med. Chem. Res.*, 2025, **34**, 172–182.
- 7 C. J. L. Murray, K. S. Ikuta, F. Sharara, L. Swetschinski, G. Robles Aguilar and A. Gray, *Lancet*, 2022, **399**, 629–655.
- 8 M. D. Vaghasiya, J. V. Mendapara, I. Ahmad, H. Patel, D. P. Rajani and P. Kumari, *J. Iran. Chem. Soc.*, 2024, **21**, 1531–1545.
- 9 A. R. Zala, D. P. Rajani and P. Kumari, *J. Biochem. Mol. Toxicol.*, 2023, **37**, e23231.
- 10 M. Magana, M. Pushpanathan, A. L. Santos, L. Leanse, M. Fernandez, A. Ioannidis, M. A. Giulianotti, Y. Apidianakis, S. Bradfute, A. L. Ferguson, A. Cherkasov, M. N. Seleem, C. Pinilla, C. de la Fuente-Nunez, T. Lazaridis, T. Dai, R. A. Houghten, R. E. W. Hancock and G. P. Tegos, *Lancet Infect. Dis.*, 2020, **20**, e216–e230.
- 11 N. Baral, D. R. Mishra, N. P. Mishra, S. Mohapatra, B. P. Raiguru, P. Panda, S. Nayak, M. Nayak and P. S. Kumar, *J. Heterocycl. Chem.*, 2019, **57**, 575–589.



- 12 M. A. Ahemad, A. Patra, L. Muduli, S. Nayak, S. Mohapatra, J. Panda and C. R. Sahoo, *Carbohydr. Res.*, 2024, **543**, 109222.
- 13 P. Panda, S. Nayak, S. Bhakta, S. Mohapatra and T. R. Murthy, *J. Chem. Sci.*, 2018, **130**, 127.
- 14 S. P. Parida, S. Mohapatra, S. Nayak, S. Mohapatra, J. Panda and C. R. Sahoo, *ChemistrySelect*, 2024, **9**, e202402223.
- 15 J. Panda, B. Brahma, S. Nayak, S. Mohapatra, B. P. Raiguru, S. Rout, S. P. Parida and K. Naithani, *J. Heterocycl. Chem.*, 2025, **62**, 99–121.
- 16 T. Das, S. Mohapatra, A. K. Pradhan and S. Nayak, *ChemistrySelect*, 2023, **8**, e202300477.
- 17 M. S. K. Youssef, A. A. O. Abeedand and T. I. El-Emary, *Heterocycl. Commun.*, 2017, **23**, 55–64.
- 18 N. Baral, S. Mohapatra, B. P. Raiguru, N. P. Mishra, P. Panda, S. Nayak, S. K. Pandey, P. S. Kumar and C. R. Sahoo, *J. Heterocycl. Chem.*, 2018, **56**, 552–565.
- 19 K. Alseud, T. Ostlund, M. Durymanov, J. Reineke and F. Halaweish, *Bioorg. Med. Chem.*, 2024, **103**, 117678.
- 20 B. S. Panda, B. Samanta, S. S. S. Sudha Ambadipudi, S. Nayak, L. V. Nayak, S. Ramakrishna, S. Mohapatra, P. M. Behera and L. Samanta, *ChemistrySelect*, 2024, **9**, e202400115.
- 21 S. Ghomashi, R. Ghomashi and M. S. Damavandi, *Sci. Rep.*, 2024, **14**, 12878.
- 22 N. P. Mishra, S. Mohapatra, C. R. Sahoo, B. P. Raiguru, S. Nayak, S. Jena and R. N. Padhy, *J. Mol. Struct.*, 2021, **1246**, 131183.
- 23 D. R. Mishra, B. S. Panda, S. Nayak, N. K. Rauta, S. Mohapatra, C. R. Sahoo and R. N. Padhy, *Tetrahedron*, 2022, **124**, 133015.
- 24 L. Xiao, D. T. Shen, W. X. Zou, J. L. Song, J. Wei, X. Liu, S. S. Zhang and L. Zhanga, *Adv. Synth. Catal.*, 2024, **366**, 3646–3652.
- 25 J. E. Barker, J. D. Tibbetts, C. T. J. Ferguson, Y. Xie and R. K. O'Reilly, *Angew. Chem., Int. Ed.*, 2024, **63**, e202410550.
- 26 M. S. Sherikar and K. R. h Prabhu, *Org. Lett.*, 2019, **21**, 4525–4530.
- 27 (a) S. G. Stewart, L. A. Ho, M. E. Polomska, A. Percival and G. C. T. Yeoh, *ChemMedChem*, 2009, **4**, 1657–1667; (b) Q. Guan, D. Zuo, N. Jiang, H. Qi, Y. Zhai, Z. Bai, D. Feng, L. Yang, M. Jiang, K. Bao, C. Li, Y. Wu and W. Zhang, *Org. Lett.*, 2019, **21**, 4525–4530.
- 28 S. K. Ko, H. J. Jang, E. Kim and S. B. Park, *Chem. Commun.*, 2006, 2962–2964.
- 29 S. Oh, H. J. Nam, J. Park, S. H. Beak and S. B. Park, *ChemMedChem*, 2010, **5**, 529–533.
- 30 S. Oh, S. J. Kim, J. H. Hwang, H. Y. Lee, M. J. Ryu, J. Park, S. J. Kim, Y. S. Jo, Y. K. Kim, C. H. Lee, K. R. Kweon, M. Shong and S. B. Park, *J. Med. Chem.*, 2010, **53**, 7405–7413.
- 31 D. Ashok, R. S. Kumar, D. M. Gandhi and A. Jayashree, *Russ. J. Gen. Chem.*, 2016, **86**, 1396–1404.
- 32 D. Ashok, R. S. Kumar, D. M. Gandhi, M. Sarasija, A. Jayashree and S. Adam, *Heterocycl. Commun.*, 2016, **22**, 363–368.
- 33 C. D. Gabbutt, D. J. Hartley, J. D. Hepworth, B. M. Heron, M. Kanjia and M. M. Rahman, *Tetrahedron*, 1994, **50**, 2507–2522.
- 34 R. Singh and G. Panda, *RSC Adv.*, 2013, **3**, 19533–19544.
- 35 R. Singh, M. K. Parai, S. Mondal and G. Panda, *Synth. Commun.*, 2013, **43**, 253–259.
- 36 R. Singh and G. Panda, *Org. Biomol. Chem.*, 2011, **9**(13), 4782–4790.
- 37 P. Singh, S. K. Dinda, Shagufta and G. Panda, *RSC Adv.*, 2013, **3**, 12100–12103.
- 38 CCDC2321501 (19i) contain the supplementary crystallographic data for this paper. The data can be obtained free of charge from the Cambridge Crystallographic Data Center via <https://www.ccdc.cam.ac.uk/structures/>.
- 39 H. M. T. Albuquerque, C. M. M. Santos, C. F. R. A. C. Lima, L. M. N. B. F. Santos, J. A. S. Cavaleiro and A. M. S. Silva, *Eur. J. Org. Chem.*, 2017, **2017**, 87–101.
- 40 U. Norinder and C. A. Bergstrom, *ChemMedChem*, **1**, 920–937.
- 41 T. Aycan, F. Öztürk and T. Doruk, *J. Mol. Struct.*, 2024, **1306**, 137865.
- 42 E. Lipinski, *Semitic Languages: Outline of a Comparative Grammar* BIUX'X@ Peeters, Publisher, Leuven, Belgium, 2001.
- 43 C. R. Sahoo, S. K. Paidesetty and R. N. Padhy, *Indian J. Pharm. Educ. Res.*, 2020, **54**, 669–675.
- 44 S. Mamidala, R. K. Aravilli, G. Ramesh, S. Khajavali, R. Chedupaka, V. Manga and R. R. Vedula, *J. Mol. Struct.*, 2021, **1236**, 130356.
- 45 B. M. Mlodawska, M. Jelen, E. Martula and R. Korlacki, *Int. J. Mol. Sci.*, 2023, **24**, 6970.
- 46 P. Banerjee, A. O. Eckert, A. K. Schrey and R. Preissner, *Nucleic Acids Res.*, 2018, **46**, W257–W263.
- 47 C. O. Nnadi, L. M. U. Ozioko, G. C. Eneje, C. M. Onah and W. O. Obonga, *Trop. J. Pharm. Res.*, 2020, **19**, 2369–2375.
- 48 S. Sestito, A. Bacci, S. Chiarugi, M. Runfola, F. Gado, E. Margheritis, S. Gul, M. E. Riveiro, R. Vazquez, S. Huguet and C. Manera, *Eur. J. Med. Chem.*, 2021, **226**, 113895.
- 49 M. S. Musa, M. S. Miah, Y. A. Munni, M. A. M. Patwary, M. Kazi and M. M. Matin, *RSC Adv.*, 2024, **14**, 30469–30481.
- 50 R. Roy, S. Rakshit, T. Bhowmik, S. Khan, A. Ghatak and S. Bhar, *J. Org. Chem.*, 2014, **79**, 6603–6614.
- 51 (a) C. Ranjith, K. K. Vijayan, V. K. Praveen and N. S. S. Kumar, *Spectrochim. Acta*, 2010, **75**, 1610–1616; (b) X. Yi, J. Zhao, W. Wu, D. Huang, S. Ji and J. Sun, *Dalton Trans.*, 2012, **41**, 8931–8940; (c) J. Sun, J. Zhao, H. Guo and W. Wu, *Chem. Commun.*, 2012, **48**, 4169–4171; (d) X. Yi, P. Yang, D. Huang and J. Zhao, *Dyes Pigm.*, 2013, **96**, 104–115; (e) K. H. Lee, M. H. Park, B. M. Seo, J. H. Seo, Y. K. Kim and S. S. Yoon, *Mol. Cryst. Liq. Cryst.*, 2011, **550**, 260–269; (f) A. Kobayashi, K. Takehira, T. Yoshihara, S. Uchiyama and S. Tobita, *Photochem. Photobiol. Sci.*, 2012, **11**, 1368–1376; (g) M. Wei, P. Yin, Y. Shen, L. Zhang, J. Deng, S. Xue, H. Li, B. Guo, Y. Zhang and S. Yao, *Chem. Commun.*, 2013, **49**, 4640–4642.
- 52 T. Lu, B. Wang, W. Chang, L. Liu and J. Li, *J. Org. Chem.*, 2023, **88**, 818–827.





- 53 S. P. Parida, A. Bhuyan, P. P. Dash, D. Mohanta, A. Pati, S. Swain, M. Palsaniya, M. Das and B. K. Kundu, *J. Clin. Trials*, 2021, **4**, 257–266.
- 54 M. Palsaniya, B. Patel, N. Panigrahi, D. Mohanta, S. P. Parida, D. K. Patel, M. Das and B. K. Kundu, *J. Biomed. Res. Environ. Sci.*, 2021, **2**, 383–391.
- 55 C. R. Sahoo, S. K. Paidesetty, B. Dehury and R. N. Padhy, *J. Biomol. Struct. Dyn.*, 2024, **42**, 2539–2549.
- 56 A. Daina, O. Michielin and V. Zoete, *Sci. Rep.*, 2017, **7**, 42717.
- 57 C. A. Lipinski, F. Lombardo, B. W. Dominy and P. J. Feeney, *Adv. Drug Delivery Rev.*, 2012, **64**, 3–26.
- 58 H. M. Faidallah and S. A. F. Rostom, *Arch. Pharm.*, 2017, **350**, 1700025.
- 59 T. Behera, S. Sethi, J. Rout, B. P. Bag and N. Behera, *Phys. Chem. Chem. Phys.*, 2024, **26**, 26431.

